STRUCTURAL INVESTIGATION AND WETTABILITY OF PVD TiN COATED CoCrMo ORTHOPEDIC ALLOY

A Thesis Submitted to
the Graduate School of Engineering and Sciences of
İzmir Institute of Technology
in Partial Fulfillment of the Requirements for the Degree of

MASTER OF SCIENCE

in Physics

by
Özlem ÇAĞLAR

July 2007
İZMİR

We approve the thesis of **Özlem ÇAĞLAR**

Date of Signature

…… **11 July 2007**
Prof. Dr. Orhan ÖZTÜRK
Supervisor
Department of Physics
İzmir Institute of Technology

…… **11 July 2007**
Assoc. Prof. Dr. Hürriyet POLAT
Co-Supervisor
Department of Chemistry
İzmir Institute of Technology

…… **11 July 2007**
Prof. Dr. Ahmet ÖZTARHAN
Department of Bioengineering
Ege University

…… **11 July 2007**
Assoc. Prof. Dr. Funda TIHMINLIOĞLU
Department of Chemical Engineering
İzmir Institute of Technology

…… **11 July 2007**
Assist. Prof. Dr. Enver TARHAN
Department of Physics
İzmir Institute of Technology

…… **11 July 2007**
Assist. Prof. Dr. Yusuf SELAMET
Head of Department
İzmir Institute of Technology

…….
Prof. Dr. Barış ÖZERDEM
Head of the Graduate School

ACKNOWLEDGMENTS

I would like to recognize Prof. Dr. Orhan Öztürk for his constant insightful advice and guidance. He has always been a great source of stability and encouragement, and I appreciate the efforts that he has made in my personal development as a researcher and numerous technical discussions required by this study.

I am very grateful to my co-advisor, Assoc. Prof. Hürriyet Polat, for her encouragement and valuable discussions related to wettability phenomena.

I am very thankful to Mr. Alptekin Aydın and Mr. Sinan Çetiner of HIPOKRAT A.Ş. for providing the medical grade CoCrMo alloy materials.

I would like to thank to Prof. Dr. Ahmet Öztarhan of Yüzey Teknolojileri Corporation for carrying out the TiN deposition of the CoCrMo specimens.

My other big "Thank you!" is for the staff of Center for Material Research of İzmir Institute of Technology for their contribution. Special thanks go to research assistants Ms. Demet Erdoğan and Ms. Mürşide Kes for helping prepare of simulated body fluid and with pH measurements. I would like to thank to Serdal Okur for polishing some CoCrMo alloy materials and for performing AFM measurements and analysis on TiN coated and uncoated CoCrMo alloy surfaces.

I am also grateful to my friends; Mine Kalkancı, Semra Gül and Barış Yeşildağ who have contributed to my experience, knowledge in science and for their encouragement, my colleagues for their support and sympathy.

Last but not least, thanks to my family, for their support, understanding and love. How little is my gratitude in comparison to their contributions.

ABSTRACT

STRUCTURAL INVESTIGATION AND WETTABILITY OF PVD TiN COATED CoCrMo ORTHOPEDIC ALLOY

Wettability, defined as the ability of any solid surface to be wetted when in contact with a liquid, is one of the most important properties of biomaterials since highly wettable surfaces are expected to disclose better adhesion of the cells. The wettability characteristics of a biomaterial's surface can be improved by surface modification techniques.

In this study, wettability characteristics of TiN coated CoCrMo orthopedic alloy materials were investigated. CoCrMo alloys were coated with TiN using physical vapor deposition (PVD) technique at 550 ºC for 6 h. The TiN coated layer microstructure, roughness, thickness, and composition were studied by X-ray diffraction (XRD), atomic force microscopy (AFM) and scanning electron microscope (SEM). Wetting studies involved contact angle and surface tension measurements using distilled water and simulated body fluid (SBF) as test liquids. The contact angles of the coated and uncoated CoCrMo alloys were investigated by the sessile drop method and the surface tension of the test liquids was measured by the ring method.

The XRD results show the PVD coated TiN films had (111) preferred orientation, while the SEM analysis indicated quite uniform TiN coated layers (about 3 μm thick) with a columnar growth mode. The AFM results indicated much higher roughness values for the TiN coated surfaces compared to the uncoated ones. The experimental results show the contact angle values for the TiN coated samples is lower than the uncoated ones suggesting better wetting for the coated layer. Based on the contact angle and the surface tension values, the work of adhesion values were estimated and it was found that the TiN coated layers has better adhesion ability compared to the uncoated CoCrMo alloy. The lower contact angles for the TiN coated samples were attributed mainly to the rougher surfaces associated with the TiN coated surfaces in comparison with the relatively smooth surface of the uncoated samples. Also, based on the EDX analysis results, the surface oxygen content on the coated surface may be another factor contributing to the better wettability characteristics of the TiN coated CoCrMo alloy compared to the uncoated alloy.

ÖZET

PVD TiN KAPLANMIŞ CoCrMo ORTOPEDİK ALAŞIMININ YAPISAL İNCELENMESİ VE ISLANABİLİRLİĞİ

Herhangi bir katı yüzeyin sıvı ile temasa geçtiğinde ıslanma niteliği olarak tanımlanan ıslanabilirlik, yüksek oranda ıslanabilen yüzeylerin hücre tutunmasının iyi olması gereği dolayısıyla biyomalzemelerin en önemli özelliklerinden biridir. Bir biyomalzeme yüzeyinin ıslanabilirlik karakteristikleri yüzey modifikasyon teknikleri ile geliştirilebilir.

Bu çalışmada, TiN kaplanmış CoCrMo ortopedik alaşım malzemelerinin ıslanabilirlik karakteristikleri incelendi. CoCrMo alaşımları 550 ºC'de 6 saat süre ile PVD kullanarak kaplandı. TiN kaplı tabakanın mikroyapısı, pürüzlülüğü, kalınlığı ve kompozisyonu XRD, AFM ve SEM ile çalışıldı. Islanma çalışmaları, kontak açısı ve yüzey gerilim ölçümleri test sıvısı olarak saf su ve simule vücut sıvısı kullanılarak yapıldı. Kaplanmış ve kaplanmamış CoCrMo alaşımlarının kontak açısı sesil damla metodu ile incelendi ve test sıvılarının yüzey gerilimi değerleri halka metodu ile ölçüldü.

SEM analizleri, kolon büyütme ile düzgün TiN kaplanmış tabakaları göstermişken; XRD sonuçları, PVD kaplı TiN filmlerinin (111) oryantasyonuna sahip olduğunu gösterir. AFM sonuçları, kaplanmamış yüzeylerle kıyaslandığında, TiN kaplı yüzeyler için daha yüksek pürüzlülük değerlerini göstermiştir. Deneysel sonuçların TiN kaplanmış örnekler için kontak açısı değerlerinin kaplanmamışlardan daha düşük olduğunu göstermesi, kaplanmış tabakanın daha iyi ıslandığı fikrini oluşturuyor. Kontak açısı ve yüzey gerilim değerlerine dayanarak adezyon enerjisi değerleri hesaplandı; ve TiN kaplı tabakaların kaplanmamış CoCrMo alaşımı ile kıyaslandığında daha iyi tutunabilme niteliğine sahip olduğu bulundu. Kaplanmamış örneklerin düz yüzeyleri ile kıyaslandığında, TiN kaplı örneklerin kontak açılarının düşüklüğü kaplanmış yüzeylerin daha pürüzlü olmasına bağlandı. Ayrıca, EDX analiz sonuçlarına göre kaplanmış ve kaplanmamış alaşımlar karşılaştırıldığında, daha iyi ıslanabilirlik karakteristiklerine sahip TiN kaplı CoCrMo alaşımını etkileyen diğer bir faktörün de yüzey oksijen içeriği olabileceği kanaatine varılmıştır.

TABLE OF CONTENTS

LIST OF FIGURES

LIST OF TABLES

CHAPTER 1

INTRODUCTION

1.1. General Background

CoCrMo alloys are metallic biomaterials. They are widely used as orthopedic implant materials in clinical practice such as hip joint replacement. Total hip joint prosthesis mainly consists of two elements: a stem implanted into the thigh bone or femur and an acetabular cup fixed in the pelvis. Figure 1.1 shows the various components of a total hip replacement. The femoral stem fits down into femur. The ball on top of the femoral stem which is called the femoral head fits into the hip and joint in the pelvis. An ultra high molecular weight polyethylene (UHMWPE) liner inserts into the acetabular cup (shell) and provides the articulating surface for the femoral head (Duisabeau et al. 2004, Long et al. 1998). The two elements of the hip implant have been made using a variety of materials such as metals, ceramics, polymers and composites.

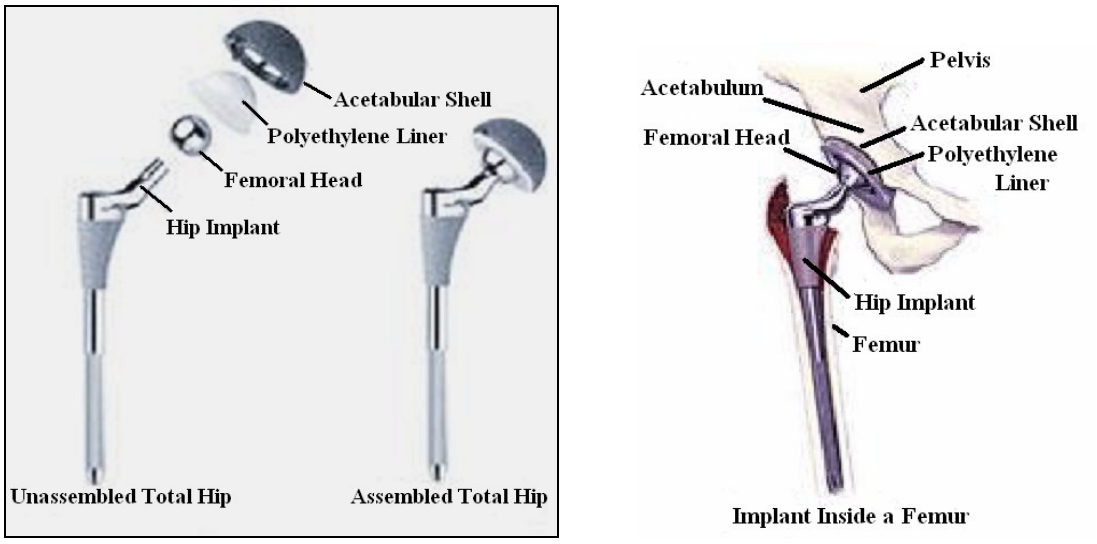

Figure 1.1. The picture shows the various components of total hip joint prosthesis. The left one represents components of an actual hip implant (Source: WEB_6).

It is obvious that implants are placed in vivo and surrounded by biological fluids within the human body. However, the human body fluid containing water, salt, dissolved oxygen, bacteria, proteins besides the various ions such as chloride and hydroxide means very aggressive environment for implants which are biomaterials made from metals and/or in combination with other materials. That's why; an ideal material or material combination to be used within such an environment should have the following characteristics:

1. Biocompatible chemical composition to avoid adverse tissue reaction and an inflammatory or toxic response over an acceptable tolerable level,

2. Appropriate mechanical properties which are closest to bone;

i. An excellent resistance to corrosion (degradation) in the human body environment,

ii. Acceptable strength to sustain the cyclic loading endured by the joint,

iii. A low modulus to minimize bone resorption and

iv. A high wear resistance to minimize the wear debris generation.

3. In addition, manufacturing and processing methods have to be economically viable (Katti 2004).

CoCrMo alloys used as biomaterials are accepted since they satisfy most of the characteristics mentioned above. That is, they are known as highly biocompatible materials involving surface compatibility, mechanical compatibility and osteocompatibility.

Surface compatibility of CoCrMo alloys arise from basic compatible chemical properties of the materials with inside of body environment;

i. Causing no toxic or allergic inflammatory response,

ii. Not stimulating changes in plasma proteins and enzymes or causing immunological reaction,

iii. Not leading to carcinogenic or mutagenic effects.

Mechanical compatibility of CoCrMo alloy is related with its properties of being non magnetic, wear-resistant and corrosion-resistant.

Excellent corrosion resistance of the material arises from the presence of an extremely thin passive oxide film that spontaneously forms on the alloy surface. On exposure to air, the oxide layer formed spontaneously on the surface of CoCrMo alloy. XPS analysis reveals that its composition is predominantly Cr_2O_3 oxide with some minor contribution from Co and Mo oxide. The calculated thickness is a few

nanometers according to (Milošev et al. 2003). These films also form on the surfaces of other metallic biomaterials such as stainless steels, titanium and its alloys. Furthermore, they serve as a barrier to corrosion processes in alloy systems that would otherwise experience very high corrosion rates. In the other words, in the absence of passive films, since the driving force for corrosion of metallic orthopedic implant alloys is very high, corrosion rates would also be high. The integrity of passive oxide films provides the chemical and mechanical stability of orthopedic implants.

Osteocompatibility of CoCrMo alloys is accepted as satisfactory in term of being implant material. This means that the material is habitable enough especially for bone-forming cells (osteoblasts) that they can colonize on the implant surface and synthesize new bone tissue. CoCrMo alloys make positive responses from osteoblasts, including increased initial cell adhesion, proliferation, and differentiation from non calcium-depositing to calcium-depositing cells (Sato et al. 2004)

1.2. Physical Vapour Deposition Coating

Vapour deposited coatings are widely used in enhancing mechanical and tribological properties such as wear, friction and hardness by altering the surface properties of materials.

The vapour deposition processes consist of two main categories: physical vapour deposition (PVD) and chemical vapour deposition (CVD) processes, which comprise various subcategories. The major techniques for deposition processes are based on sputtering, evaporation and ion plating (Vencovsky et al. 1998). The deposition species are transferred and deposited in the form of particular atoms and molecules. PVD or CVD, each one has its own well-defined technical and/or economic advantages and disadvantages.

PVD and CVD techniques are industrially used to improve wear, corrosion resistances and reduced friction. Titanium nitride (TiN) and chromium nitride (CrN) are widely used for this type of material improvement. These nitrides having an excellent combination of performance properties are used in cutting tools, steels and medical devices. TiN is used mostly in medical devices and metallic biomaterials due to safety and biocompatibility. TiN, which is in ceramic nature, exhibits greater inertness to the corrosive body fluids than the metallic substrates.

The other property of TiN lies in its high hardness and its remarkable resistance to wear and corrosion that allow its use in producing high performance coatings and cutting tools. Examples proving the arguments can be given as;

i. TiN is also a suitable material for orthopedic implants because of its intrinsic biocompatibility.

ii. It is used as a coating for the heads of hip prostheses to improve their wear and fatigue resistance.

iii. TiN is preferred in hard coating of dental implants and dental surgery tools (Piscanec et al. 2004).

Femoral heads for hip replacements and wear plates in knee replacements have been constructed using ceramics. In hip replacements, the ceramic (TiN) femoral head is used in connective with a metallic femoral stem and an acetabular cup made from UHMWPE for the opposing articulating surface. When the wear rate is compared, it was observed that wear rate for TiN on UHMWPE was 20 times less than that for metal on UHMWPE. That is, comparison proved that TiN combination is far superior in producing less wear debris (Katti 2004).

It was observed clear advantages for TiN coatings by a reactive magnetron sputtering in terms of higher hardness, toughness, wear properties and good adhesion strength (Li et al. 2001 and Chenglong et al. 2005). Thus, sputter technique will be used in this study.

1.2.1. Sputter Technique

Sputter coating, which takes place at sub-atmospheric pressures, is a physical vapour deposition (PVD) process. The surface, which is called as substrate, to be coated and the coating material called as target are arranged in the vacuum chamber, as shown in Fig. 1.2, or they may be moving past each other in case of larger substrates.

In the surface coating, the high voltage applied between substrate and target ionizes the gas (usually argon, but other gases are possible) in the chamber until a plasma is ignited. In practice, voltages are used which are direct current (DC) and radio frequency (RF) and target usually being cathode. When it is positive charge, the plasma ions are accelerated towards the cathode, and hitting the cathode surface. This causes

plasma ions dislocate atoms from the target surface (indicated by grey circles in Fig. 1.2). These atoms can in turn be deposited on other parts of the surface.

Reacting the ions and atoms in the vacuum chamber, reactive gases N_2, are available in the vacuum chamber in addition to the inert plasma gas and this is called as ‘‘reactive sputtering’’. If the desired final surface film does not adhere well, the substrate can be precoated with another material. The advantages of sputter coatings are the hard and generally very adhesive films (Santos et al. 2004).

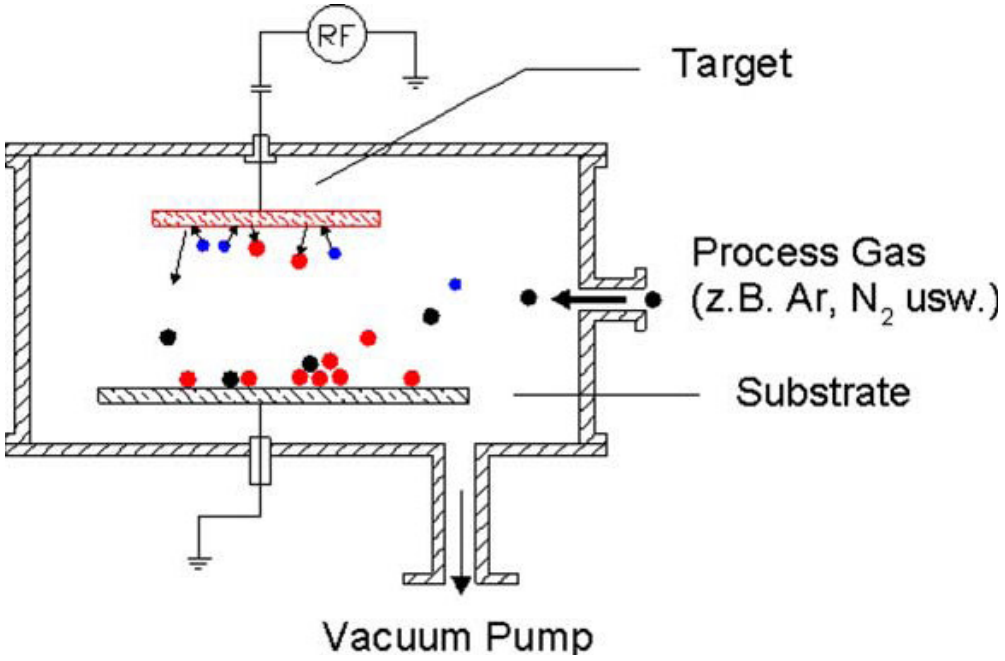

Figure 1.2. Schematic representation of sputtering equipment.
(Source: Santos et al. 2004)

In order to have better surface, mechanical and osteo compatibilities for CoCrMo alloys with its surroundings in vivo, wettability issue of the material should be well understood. Because the better wetting characteristics of prosthetic materials lead to

i. The adhesion of osteoblasts on the surface substrate (Hao et al. 2006) and

ii. The friction and wear processes (Widmer et al. 2001, Davidson 1993, Borruto et al. 1998 and Gispert et al. 2006).

1.3. Purpose of This Work

The aim of this study is to improve our understanding of surface modification of CoCrMo alloy and TiN coated CoCrMo alloy. In particular, structural and the wettability characterization of PVD TiN coated CoCrMo orthopedic alloy are aimed to be searched and specified. It will be discussed that TiN coating (via PVD) on CoCrMo is an advantage for the total hip replacement.

This will be accomplished by experimental characterization of the near surface crystal structures by using;

1. X-ray diffraction (XRD)

2. Scanning Electron Microscopy (SEM). SEM will be used

i. To examine the surface morphology of as-polished and TiN coated samples by secondary electron mode,

ii. To observe the TiN coating layer thicknesses by cross sectional electron microscopy mode and

iii. To research the surface elements of TiN coated samples by energy dispersive x-ray spectroscopy (EDX).

3. Atomic Force Microscopy (AFM) in order to investigate

i. The surface morphology,

ii. The mean surface roughness (Ra) and

iii. Three-dimensional topology of the surface of TiN-coated and uncoated specimens.

4. Wettability analysis for CoCrMo substrate and TiN coated CoCrMo alloys by

i. Measuring contact angle and

ii. Measuring surface tension by using ultrapure water (25 ° C and 37 ° C) and simulated body fluid (37 ° C).

ii. To calculate the adhesion work to determine the surface wettability.

CHAPTER 2

WETTING PHENOMENA

2.1. Wettability Issue

Even if the general description of "wettability" implies "the quality or state of being wettable or the degree to which something can be wet", scientific definition is more specific. Wettability is specifically defined as the ability of any solid surface to be wetted when in contact with a liquid whose adhesion forces are more than cohesive forces, so that liquid spreads over the surface of the solid. In other words, a solid surface should be hydrophilic enough be accepted as having wettability character.

Wettability is one of the most important properties of biomaterials in addition to the possibility of modification being essential for their surface engineering. It is mainly caused by hydrophilic properties of the substances. This property gives several advantageous in use of materials designed to be interfaced with a human body. For example, in a situation to form permanent associations with surrounding cells, the hydrophilic properties are advantageous since water-based body fluids are dominant vector of cells transport. Highly wettable surfaces are thus expected to disclose better adhesion of the cells (Jagielski et al. 2006 and Azevedo et al. 2005).

In the case of mechanical parts, such as elements of hip joint prosthesis, the situation about wettability is much more complex. Complexity is mainly derived from the possibility that unwanted process of the build-up of the cells between the sliding surfaces occurs in a water-based medium needed to provide sliding. Thus, it is of prime importance to study the wear and friction processes in water based solutions as body fluid. When the load of the friction pair is low, that is typical for bioimplants, the liquid film remains between the two sliding surfaces. In fact, the friction becomes a three body process involving two parts of the prosthesis and a liquid layer between them. In such a configuration, the main friction forces are not related with the interactions between two surfaces of the prosthesis, but they arise from the cutting of adhesive bonds between one of the surfaces and the liquid. The adhesion between material and the liquid is directly proportional to the wettability of the surface; the lower is the adhesion force, the higher is hydrophobicity of the surface. In addition, the liquid layer between the surfaces in

motion persists more when at least one of these surfaces is hydrophilic (Jagielski et al. 2006). In order to have reduction of the friction factor and the wear using water lubrication the best coupling is made of hydrophilic-hydrophobic materials (Borruto et al. 1998). The possibility of tailoring of wettability appears thus as very promising and prospective option in surface modification of biomaterials.

Biocompatible or biotechnological materials need hydrophilic property as the surface characteristics. In details, controllability of hydrophilic or hydrophobic properties is very important technology for biomaterials. Besides, implant system must present excellent adhesion and very good mechanical characteristics (Okabe et al. 2005 and Azevedo et al. 2005).

The surface wettability of the prosthetic materials affects friction and wear. This influence on the friction behaviour of a tribological system and gives an indication of its biotolerance. The more wettable the material is the better the human body tolerates it. Clearly, techniques to control the wettability characteristics of a biomaterial's surface are of great interest (Annarelli et al. 1999 and Hao et al. 2005). An alternative approach to prevent friction and to increase the wettability is coating. The coating by physical vapour deposition (PVD) is expected to result in enhanced wettability and wear resistances for CoCrMo orthopedic alloys.

2.2. Wetting

Wettability is often called as the affinity that a liquid has for a solid surface. The affinity is used in order to control adhesion and motion of fluids in countless applications (Robinson et al. 2006). For a surface to be wetted, a liquid (usually water) has to spread over it, in spite of the liquid's tendency to minimize its surface area. In nature, objects tend to change in the way that they minimize their total energy (Web_2).

Wetting is related with the relative strength of the adhesive and cohesive forces. Cohesive forces hold the particles of the liquid together. Adhesive force is the force of attraction between the liquid and the surface to be wet. If the adhesive forces are greater than the cohesive forces, the liquid will wet the surface. On the contrary, if the cohesive forces are greater than the adhesive forces, the liquid will bead up and will not spread over or wet the surface. Wettability is also expressed in terms of hydrophilic and hydrophobic characteristics of substances. Substances having a strong affinity for water

are called hydrophilic and water will spread easily on these surfaces. But, for the hydrophobic substances, water beads up on and do not spread over the surface of it (WEB_2).

The extent or a degree of being wet for a solid by a liquid can be determined by examining the surface tension and the shape that a drop makes with the solid surface. The contact angle is a good indicator for examination of the shape that a liquid drop form with solid surface and measurement of it inside the liquid drop provides a good way in specifying the degree of wetting (WEB_2).

2.3. Contact Angle

The contact angle formed when a drop of water is placed on a surface is a common way for measurement of hydrophobicity. It is an angle between the solid–liquid and liquid–vapour interfaces of a droplet on a surface. An example angle is shown as θ in Fig. 2.1. The contact angle θ between the solid–liquid and liquid–vapour interface indicates how much the water likes the solid surface as compared to the air. A small contact angle (much less than 90°) indicates a hydrophilic surface, while a contact angle approaching or larger than 90° indicates a hydrophobic surface (Robinson et al. 2006).

On the other hand, the contact angle characterizes the surface of different materials and they are defined wettable (highly hydrophilic $0° \leq \theta \leq 45°$) or not wettable (highly hydrophobic $90° \leq \theta \leq 180°$), the other values are called basically hydrophobic according to (Zettlemoyer 1960, Melrose 1968 and Borruto et al. 1998).

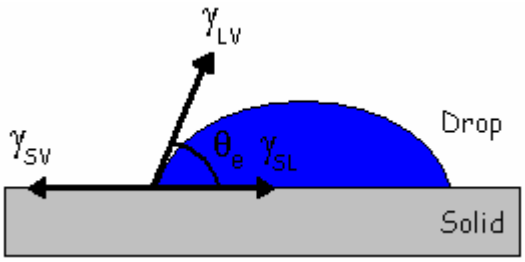

Figure 2.1. Water drop on solid surface with surface tensions indicated as arrows originating at the 3-phase interface line. The reflection of the drop can be seen under the base line (Source: WEB_9).

The contact angle of a drop (Fig. 2.1) deposited on a solid is given by the Young's equation.

$$\cos \theta = (\gamma_{sv} - \gamma_{sl}) / \gamma_{lv} \qquad 2.1$$

γ is the surface tension or surface energy which is energy per unit surface area of the interface, subletters *s, l, v* stand for the solid, liquid and vapour phases.

Young's derivation is a straightforward equation in defining the balance between three phases. It simply indicates that each surface tension of phases acts to reduce the corresponding surface area and final combinations of them make balance on the solid plane with cosine of contact angle as in Eq. 2.4. It fixes in the vicinity of the contact line, where the three phases coexist (Quéré 2002).

The surface tensions in Eq. 2.4 typically vary between values of 20 and 1000 mN/m. There is no theorem forcing the ratio $(\gamma_{sv} - \gamma_{sl}) / \gamma_{lv}$ to be smaller than unity (in absolute value). Three cases appear to be particularly interesting practically (Quéré 2002):

- If $(\gamma_{sv} - \gamma_{sl})$ is equal to γ_{lv}, than contact angle is zero ($\theta = 0°$) which means the drop tends to spread completely on the solid. Conversely, when the proportion of γ_{lv} to $(\gamma_{sv} - \gamma_{sl})$ decreases, it leads θ to be closer to 90° which means hydrophobic surface. This explains why liquids of low surface tension wet most surfaces (Quéré 2002).
- If $(\gamma_{sl} - \gamma_{sv})$ is equal to γ_{lv}, than contact angle is 180° ($\theta = 180°$) which means the drop is in a pure drying (non-wetting) situation in which sits on the solid. A very simple way to observe a non-wetting situation consists of inverting the liquid and vapour phases: then, the contact angle is $\pi - \theta$, which leads to a "drying" situation (for the vapour) for $\theta = 0°$ (Quéré 2002).

By measuring the contact angles on substrate for varying liquids in both the coated and uncoated states, deeper knowledge was gained about the magnitude of wettability or hydrophilicity.

2.4. Surface Tension

The cohesive forces between molecules inside of a liquid are shared with all neighboring atoms. However, since there is no neighboring atom above the surface, this

makes nearest neighbor atoms on surface to exhibit stronger attractive forces (Fig. 2.2). This enhancement of the intermolecular attractive forces at the surface is called surface tension (WEB_3).

Since the surface molecules miss half of their attractive interactions, unbalanced forces for the molecules at the surface lead to additional energy which is known as surface energy (surface tension) as shown in Fig. 2.2. This additional energy is the fundamental reason behind liquids adjusting their shapes to expose the smallest possible area (WEB_4).

The existence of surface energy (surface tension) and the cohesion between materials are from van der Waals forces. These forces between macroscopic objects are usually attractive, but under certain circumstances they can be negative. Almost all interfacial phenomena are influenced to various extents by forces. The forces have their origin in atomic and molecular level interactions. It is due to the induced or permanent polarities created in molecules by the electric fields of neighboring molecules, or it is due to the instantaneous dipoles caused by the "positions" of the electrons around the nuclei. These forces consist of three major categories known as *Keesom* interactions (permanent dipole/permanent dipole interactions), *Debye* interactions (permanent dipole/induced dipole interactions), and *London* interactions (induced dipole/induced dipole interactions). These three interactions are known collectively as the van der Waals interactions. They play a major role in determining material properties and behavior important in surface chemistry (Hiemenz et al. 1997)

In other words, surface tension of a material is the excess energy per unit area due to the existence of the free surface. If U is accepted as the cohesion energy per molecule inside the liquid, then energy shortfall for a molecule sitting at the surface is approximately U/2. So, the surface tension is $\gamma \approx U / 2a^2$ where "a" is the size of a molecule; a^2 is the exposed area of a molecule (WEB_4).

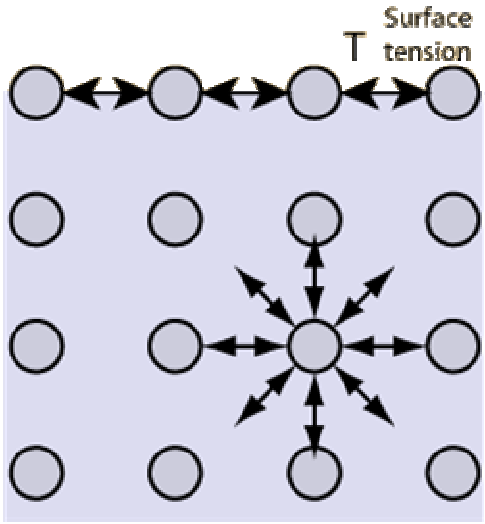

Figure 2.2. Surface tension of the molecules.
(Source: WEB_4)

Derivation of surface tension theoretically comes from knowledge of intermolecular forces. Fowkes has suggested that total free energy at a surface is the sum of contributions from the different intermolecular forces at the surface:

$$\gamma = \gamma^d + \gamma^a \qquad 2.2$$

d refers to the dispersion forces and *a* refers to scalar forces in which the combined polar interactions are dipole, induction, and hydrogen bonding (WEB_4). However, in this study total surface tension (surface energy) approach was investigated.

2.5. Work of Adhesion and Gibb's Free Energy

Significant advances have been made in the thermodynamic treatment of Gibbs free energies, largely due to the work of adhesion. For thermodynamic reactions, Gibbs free energy has to be negative to wet the surfaces. The change in Gibbs free energy dG when the drop spreads an infinitesimal amount,

$$dG = \gamma_{sl}\, dA - \gamma_{sv}\, dA - \gamma_{lv}\, dA \qquad 2.3$$

the dA is the change in the surface area of each phase boundary in contact. γ is the surface tension of the interface. These balances at the 3-phase contact line: solid–liquid γ_{sl}, solid–vapour γ_{sv} and liquid–vapour γ_{lv} (Rosen 1989).

In adhesional wetting, a liquid not originally in contact with a substrate makes contact with that substrate, and adheres to it. In this case the change in surface free energy (Gibbs free energy) is $-\Delta G = a\ (\gamma_{sv} - \gamma_{sl} + \gamma_{lv})$, where a is the surface area of the substrate in contact with (an equal) surface area of the liquid after adhesion, and the "driving force" of this type of wetting phenomenon is $(\gamma_{sv} - \gamma_{sl} + \gamma_{lv})$. This quantity is known as the work of adhesion W_a , the work required to separate unit area of liquid from the substrate (Rosen 1989):

$$W_a = \gamma_{sv} - \gamma_{sl} + \gamma_{lv} = -\Delta G \qquad 2.4$$

As it is shown in Fig. 2.1, there must be in balance between the forces of solid-liquid-air system, which are called the surface tensions. For the equilibrium conditions, the forces are determined using the equation:

$$\gamma_{sv} = \gamma_{sl} + \gamma_{lv} \cos\theta \qquad 2.5$$

In this equation γ_{lv} and θ are directly measurable, but γ_{sv} and γ_{sl} are not. When Eq. 2.4 is combined with this equation (Eq. 2.5), the work of adhesion can be calculated in the following equation:

$$W_a = \gamma_{lv} (1+\cos\theta) = -\Delta G \qquad 2.6$$

This equation shows that the methods for determining the surface free energy (ΔG) or W_a are used by measuring the value of γ_{lv} and the contact angle, θ, between the solid and liquid. Since the work of adhesion is the work per unit area of interface that must be performed to separate reversibly the two phases, it is therefore a measure of the strength of the binding between the phases (Contreras et al. 2004).

Good wetting means that the interfacial bond is energetically nearly as strong as the cohesion bond of the liquid itself. Wetting can be obtained not only in systems featuring strong liquid/solid interactions (ionic, covalent, metallic or some mixture of them), but also in systems featuring weak liquid/solid interactions (for instance van der

Waals forces) provided that liquid/liquid interactions are weak too (Eustathopoulos et al. 1999 and Contreras et al. 2004).

2.6. Literature Review

Advanced biological materials require an appropriate surface treatment ensuring the best possible interface between implant and human body and optimum functional properties (Jagielski et al. 2006). In the field of the surface modification, it is important to improve the surface properties of different materials (Tang et al. 2005). The term "surface engineering" encompasses whole techniques and processes which are utilized to induce, modify and enhance the performance, such as wear, fatigue and corrosion resistance, wettability and adhesion or biocompatibility (Škorić et al. 2004).

The work of Hao et al. investigated the surface properties of the 316LS biodegrade stainless steel following the irradiation of a CO_2 laser and a high power diode laser (HPDL), especially the modification of wettability characteristics. The results revealed that the wettability of the stainless steel improved after treatments. The determined adhesion work towards simulated physiological liquid indicated that the laser modification brought higher adhesion of biological liquids to the stainless steel (Hao et al. 2005).

According to Hao et al., the changes in surface roughness, surface oxygen content and surface energy generated by the laser treatment could be the factor influencing the wettability characteristics of the stainless steel. The roughness (Ra) results revealed that laser treatment brought about a rougher surface and a higher wettability characteristic of stainless steel samples than the smooth, untreated sample (Hao et al. 2005).

The other factors such as surface oxygen content and surface energy were active in wettability modifications. The results showed that wettability increased with surface oxygen content (Hao et al. 2005). Wettability measurements on oxidized Ti surfaces were investigated for different oxidation conditions. The wettability was influenced by the oxide layer. In the case of oxide layer existence the wettability was observed as increased (Feng et al. 1998). The resulting graded TiO_2 films can be utilized in many fields, such as the hydrophilic properties and low frictional resistance hull. These results

may serve as a guideline for preparing the surface properties of TiO_2 films, especially when the film wettability property is concerned (Wu et al. 2006).

Furthermore, the exhibited increase in the surface energy of the stainless steel after laser treatment generated the higher wettability characteristics. After CO_2 laser treatment, the stainless steel with the highest surface energy has the lowest θ with physiological test liquids and thus highest wettability characteristics (Hao et al. 2005).

Since adhesion largely depends on the surface properties of the materials, it is necessary to modify near-surface region without affecting the bulk properties of the material (Tang et al. 2005). In case of problems related to cell adhesion or wettability, the modification of the uppermost surface layer is also sufficient. The treatment can be selectively applied only to defined areas of the objects. This option is particularly interesting when the chemical inertness of material is of prime importance (Jagielski et al. 2006).

The film deposition, which is a kind of surface treatment application, process exerts a number of effects such as crystallographic orientation, morphology, topography, wettability of the films. However, the adhesion can be substantially improved by coating on various substrates (Mogensen et al. 1998, Ensinger 1998 and Škorić et al. 2004). For different materials thin layers to be applied by PVD technology are not only protect against wear and corrosion but can also help reduce friction. The wetting behavior of the material surface is influenced by the lubricant; this is due to the differences in surface energy of PVD-coated material surfaces (Lugscheider et al. 2003).

In the study of Chenglong et al., the protective films as TiN films and Ti/TiN multilayered coatings on surgical AISI316L stainless steel improved the corrosion resistance and the protein adsorption (Chenglong et al. 2005). Also when the glass substrate was deposited by TiN using DC pulsed magnetron system, the surface chemistry changed and improved the adhesion for cells on the surfaces (Cyster et al. 2003).

In this study, the influence on the wettability by plasma vapor deposition coating surface treatment method will be investigated to improve the adhesion properties and wear-friction resistance of CoCrMo orthopedic alloys.

CHAPTER 3

EXPERIMENTAL METHODS

3.1. Materials

Cobalt-chromium-molybdenum (CoCrMo) alloy was the base material on which TiN was deposited. It has nominal composition of 1 % Ni, 0.75 % Fe, 1.0 % Mn, 1.0 % Si, 0.35 % C, 0.25 % N, 5 % Mo, 26 % Cr and balance Co (all in wt %), as specified in ISO 5832-12. The specimen geometry was designed as a disk, having 3 cm diameter and the thickness of 0.3 cm. The average grain size for the specimens of this study, obtained by metallography, was ~ 5 to 15 μm (Öztürk et al. 2006). Before the coating, all the specimens were polished to mirror like quality, with a mean surface roughness of about 5 nm.

3.2. Test Liquids

The contact angles (θ) were measured using two kinds of liquid, one is ultrapure water (distilled water) and the other is simulated body fluid (SBF). For ultrapure water, pH value is 7, the contact angle by sessile drop method was observed at two different temperatures 25°C and 37°C, respectively.

SBF is generally saturated solution whose ion concentrations and pH are close to those characteristic to human blood plasma. Simulated body fluid (SBF) was prepared according to procedure in the literature by dissolving reagent grade chemicals of NaCI, $NaHCO_3$, KCI, Na_2HPO_4, $MgCI_2.6H_2O$, $CaCI_2.2H_2O$ and Na_2SO_4 in autoclaved deionised water. The chemicals were added to the solution in the order they are listed. The simulated body fluid solution was buffered at physiological pH 7.4 at 37 °C with 50 mM trishydoxmethyl aminomethane $[(CH_2OH)_3CNH_2]$ (THAM) and 36.23 mM HCI acid. HCI was added before calcium chloride and THAM was the last reagent added to the solution. The amounts of reagent grade chemicals used are listed in Table 3.1.

Table 3.1. Reagents used for the preparation of SBF (pH 7.4, 1L).

Order	Reagent	Amount (g)
1	NaCl	6.547
2	$NaHCO_3$	2.268
3	KCl	0.372
4	Na_2HPO_4	0.124
5	$MgCl_2.6H_2O$	0.305
6	1M HCl	~ 40 mL
7	$CaCl_2.2H_2O$	0.368
8	Na_2SO_4	0.071
9	trishydoxmethyl	6.057

The ion concentration of the SBF and blood plasma are nearly the same. Table 3.2 shows the ion concentrations (mM) of the SBF and the human blood plasma. After preparing SBF, the contact angles were measured at 37 ° C.

Table 3.2. Ion concentration (mM) of SBF and human blood plasma.
(Source: Türkan 2004)

Ion	SBF	Human Blood Plasma
Na^+	142.0	142.0
K^+	5.0	5.0
Mg^{2+}	1.5	1.5
Ca^{2+}	2.5	2.5
Cl^-	147.8	103.0
HCO_3^-	4.2	27.0
HPO_4^{2-}	1.0	1.0
SO_4^{2-}	0.5	0.5

3.3. PVD Coating

Physical vapour deposition (PVD) method was used to deposit titanium nitride (TiN) on CoCrMo alloy substrate. The PVD was carried out by an industrial type (CC880/8 with CK288 cathode) coating machine. Before deposition, the substrates (as-polished specimens) were ultrasonically cleaned and, in situ, sputter etched in a pure argon atmosphere. The coatings were deposited from a titanium cathode material which was in an argon and nitrogen atmosphere. During the deposition only 2 of the 4 cathodes were working and they were placed as cross shaped. The coating temperature was 550 °C. The bias voltage applied to the substrate was 110 V. The deposition time was 6 hours. The chamber pressure was 0.5 mPa. Totally, 8 specimens were coated with TiN (sample no's 1; 2; 3; 4; 7; 8; 14; 15). In this study, three samples (#1, #7 and #8) were investigated.

3.4. Microstructural Characterization

Near surface crystal structures and composition of CoCrMo and TiN coated CoCrMo alloys were characterized microstructurally with the help of X-ray diffraction (XRD), scanning electron microscopy (SEM) and atomic force microscope (AFM). Surface morphology and the roughness were measured by AFM. SEM was used in two different modes: (1) scanning electron (SE), (2) energy dispersive x-ray spectroscopy (EDX), respectively. Topographic information and chemical compositions of the samples were obtained by means of SEM.

SEM was used for viewing the surfaces in details, also cross-section analysis, which was used for both measuring the thickness of the TiN coated layers and investigating the quality of the coating.

3.4.1. XRD Analysis

Because low energy x-rays are strongly absorbed in passing through solid materials, X-ray diffraction analysis can be used for characterization of the surface layers of TiN coated materials. XRD analysis gives the fundamental physical and

chemical knowledge including crystal structure identification, layer composition and thickness determination, and crystallite sizes and preferred orientation.

X-ray measurements were made with a θ/2θ diffractometer with Cu Kα x-rays (λ = 1.5404 for the 8.05 keV x-rays) from a high intensity x-ray tube (Philips X'pert). The voltage and current used were 45.0 kV and 40 mA, respectively. The data collection was made with a computer controlled system. The resultant spectrum was in the form of the scattered x-ray intensity (counts/s) versus 2θ (degrees). The presented diffractograms in this study were plotted in square root of x-ray intensity [Sqrt (x-ray intensity)] versus 2θ (degrees) to reveal weaker patterns much more clearly. The 2θ range for the specimens of this study was 30 to 100 degrees, which gives a scan time of about 1 hour 56 minutes for the step widths and times used in this experiment (0.03° and 10 s, respectively).

The effective depth probed by Cu Kα x-ray was such that it allowed the characterization of the TiN coated layer as well as the substrate phase. The effective depth was calculated by the formulation of sinθ/2μ (Cullity 1978) where μ is the effective linear absorption coefficient that approximately equals to 2540 cm^{-1} for CoCrMo alloy used in this study (Öztürk et al. 2006). Bragg Brentano (θ/2θ) was facilitated during the XRD measurements.

3.4.1.1. Bragg-Brentano Method (θ/2θ)

The method is generally known as powder method. Because the system always detects the scattered x-rays at a diffraction angle which equals to the angle of x-rays incident of the surface, it can be defined as a symmetric method. The sample and the detector both move step by step during the measurement. That is, when the samples rotate at an angle (θ) the detector moves two times this angle (2θ). Therefore, always the diffracted x-rays from grains oriented parallel to the surfaces are detected in this method. Main disadvantage of this geometry is that the effective depth probed by the incident beam always changes during the scan due to the change in the angle of the incident beam. For instance, a typical scan range in 2θ for most metals is from 30 to 100 degrees. However, there is a big difference between the effective depths probed by beam at 2θ = 30 degrees and at 2θ = 100 due to the change in the incident beam angle.

As a comparison, the effective depth probed by the beam at 2θ = 100 degrees (1.4 μm) is approximately 3 times deeper than the effective depth probed by the beam at 2θ = 30 degrees (0.49 μm) (Türkan 2004).

3.4.1.2. Lattice Parameter Analysis

Lattice parameter measurements are used in many situations to characterize materials based on knowledge of the lattice parameters can provide information on the thermal properties of a material, an indirect method to determine the compositions in a solid solution, a measure of the strain state, or an analysis of the defect structure. Hence, it is important to determine the lattice structure with the highest precision. Fortunately, X-ray diffraction can supply such information to an accuracy of several significant figures if care is taken during the experiment and subsequent analysis (WEB_1).

The diffraction pattern can be indexed rather easily, if the crystal structure of a material is known. However, in order to use this indexing to compute a precise value of the lattice parameter, careful analysis of the data is required. In a cubic system (FCC- γ phase) for uncoated CoCrMo and TiN coated CoCrMo, the lattice parameter *a* are calculated by equation 3.1. Then in a hexagonal system (HCP- ε phase) for as-polished CoCrMo, the lattice parameters, *a* and *c*, are calculated by equation 3.2.

$$\sin^2 \theta = \lambda^2 (h^2 + k^2 + l^2) / 4a^2 \qquad 3.1$$

$$\sin^2 \theta = [\, \lambda^2 (h^2 + hk + k^2) / 3a^2 \,] + [\, l^2 / c^2 \,] \qquad 3.2$$

where (hkl) are the Miller indices, λ is the X-ray wavelength . If there were no systematic errors in the positions of the diffraction peaks, then there would be only random errors in the individual calculations of the lattice parameter. However, systematic errors occur for a number of reasons that require a sophisticated approach to compensate fully for such errors (WEB_1). The lattice parameters of all the samples were calculated in this study.

3.4.1.3. Grain Size Analysis of TiN Coated Layer

The peaks in the obtained XRD plots were identified by comparing the lattice parameters reported. Thus the deposited film was confirmed to be TiN coated CoCrMo with the peak corresponding to the (111) plane being the strongest one. The crystallite sizes (grain size - *D*) were estimated using the Debye–Scherrer formula;

$$D = 0{,}9\,\lambda / B \cos\theta_B \qquad 3.3$$

where λ is the X-ray wavelength, θ_B the Bragg's angle, B the full width of the diffraction line at half of the maximum intensity (Roy et al. 2002). The grain sizes of the specimens were calculated and recorded in this thesis. They were also compared with those of the SEM findings.

3.4.2. SEM Analysis

Philips XL-305 FEG Scanning Electron Microscope (SEM) was used in Secondary Electron (SE) and Energy Dispersive analysis of X-ray (EDX) modes. SEM in SE mode was used for surface morphology analysis for CoCrMo alloys and TiN deposited specimens. Cross sectional SEM analysis was done on a few selected specimens to examine the possible use of this method for measuring TiN coated layer thicknesses. Before SEM analysis, specimens were mounted in the standard bakelite material, polished (1 μm diamond) then cleaned using an ultrasonic cleaner; first in acetone, and then in ethanol.

SEM in EDX mode was also used to investigate the surface elements of specimens (TiN coated). The EDX analysis method is based on the detection of x-rays emitted during the interaction of incident electron beam with material. The emitted x-rays are characteristic to the emitter atoms or the elements. Therefore, elemental analysis determination is the main power behind the EDX.

3.4.3. Atomic Force Microscope

AFM analysis was used for surface morphology and average roughness (Ra) of as-polished and TiN coated samples. Digital Instrument MMAFM-2/1700EXL Atomic Force Microscope was used in tapping mode. Current information and scanner tips position recorded by a computer with software which is Nanoscope Program. Two different kinds of samples were investigated by AFM, one is polished substrate (CoCrMo) and the other is TiN coated CoCrMo. Before AFM analysis, specimens were cleaned using an ultrasonic cleaner; first in acetone, and then in ethanol. The average roughness (Ra) of the uncoated and the TiN coated specimens were investigated by atomic force microscopy (AFM) and recorded topographical details. All the samples were scanned by the 30x30 μm scales in 5 times, the 50x50 μm scales in 3 times, the 100x100 μm scale around different regions of the samples. In addition to these scans, TiN coated CoCrMo alloys were obtained in scales the 20x20 μm, the 10x10 μm and the 5x5 μm.

3.5. Wetting Studies

The wetting experiments were conducted using components of adhesion energy (adhesion work), which are contact angle and surface energy. To investigate the effects of coating, the contact angle (θ) and the surface energy (γ) characteristics of the as-polished CoCrMo alloys and TiN coated CoCrMo samples were measured. Two test liquids were used as a probe for surface free energy calculations: ultrapure water at 25 ° C and 37 ° C, and simulated body fluid at 37 ° C.

3.5.1. Contact Angle Methods

Contact angle (θ) measurements were carried out on as-polished and TiN coated CoCrMo alloys using distilled water and simulated body fluid (SBF). The sessile drop method by KRÜSS Contact Angle was used. Several points on whole surface of the specimens were measured as SBF and ultrapure water. Uncoated and coated samples were ultrasonically cleaned in acetone, ethanol in sequence for 10 minutes before contact angle measurements.

Contact angle of specimen surfaces was measured to estimate the characteristic of hydrophilic or hydrophobic by means of liquid drops. A liquid drop was 60 µl and the drops were uniformly dispersed on each surface by a micrometer pipette. When the drop spread over the surface of the solids, the drop size was about 5 mm in diameter. The drops were measured after 1 minute to provide the configuration between the measurements. The mean contact angle was obtained from two hundred (200) measurements for each uncoated and TiN coated CoCrMo samples, and then the frequency distributions of the measured contact angles were plotted. The averages of the contact angles and the standard deviation were calculated.

3.5.2. Surface Tension Methods

Surface energy (surface tension) of the ultrapure water and simulated body fluid at different temperatures (25 ° C and 37 ° C) were measured with KRÜSS Digital-Tensiometer K 10ST, which is used to determine the tension by the ring method. For ultrapure water at 25 ° C, ultrapure water at 37 ° C and SBF at 37 ° C, about twenty values were measured and the average was calculated for each liquid.

3.5.2.1. Surface Tension Measurements

Most tensiometers measure the surface or interfacial tension by the help of an optimally wettable ring or plate probe suspended from a precision balance. Liquid to be measured is brought into contact with the probe by a height-adjustable sample carrier. A force acts on the balance as soon as the probe touches the surface. As circumference of ring probe or length of plate probe is known, the interfacial or surface tension is calculated by using the force measured. A further specific requirement for the probe is that it must have a very high surface energy to keep the liquid well. That's why, a platinum-iridium alloy is used for the ring (WEB_5).

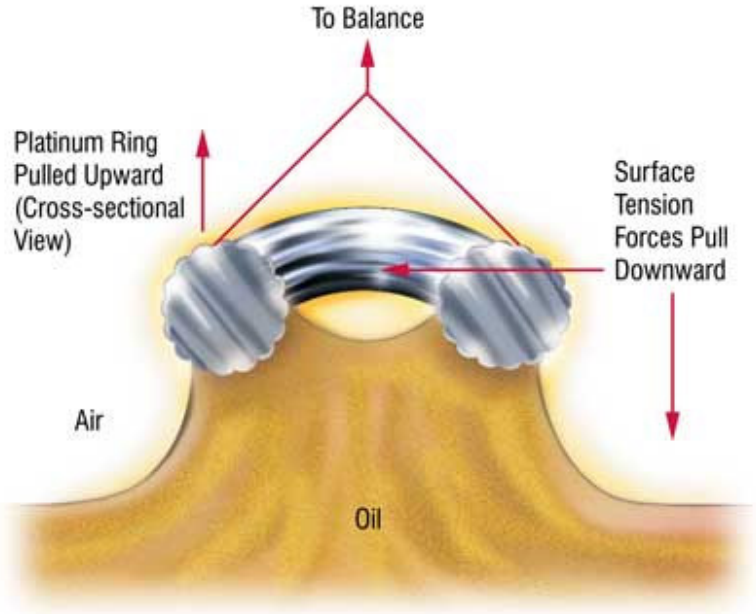

Figure 3.1. The platinum ring is the wettable probe to suspend from a precision balance. (Source: WEB_7)

3.5.2.1.1. The Ring Method

The ring method was the first method developed. That is why many of the values for interfacial and surface tension given in the literature are the results of the ring method. In the ring method, the liquid is first raised until contact with the surface is registered. Then, the liquid is lowered so that the liquid film produced beneath the ring is stretched (WEB_5).

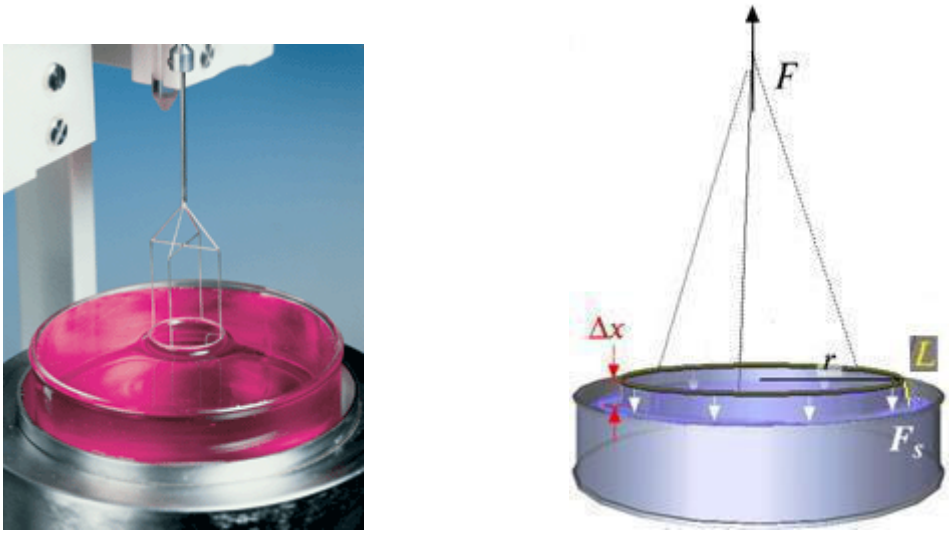

(a) (b)

Figure 3.2. (a) Measuring the surface tension by the ring method; (b) the components of the calculating the surface tension (Source: WEB_8).

In practice the distance is first increased until the area of maximum force is passed through. Then, the process is repeated by moving sample vessel containing the liquid back so that the maximum point is passed through a second time.

The maximum force can be only determined exactly on this return movement and it is used to calculate the tension. The calculation is made according to the following equation:

$$\gamma = (F - F_s) / \Delta x \qquad 3.4$$

$$\Delta x = L \cos \theta \qquad 3.5$$

Where; γ = surface or interfacial tension,

F = maximum force,

F_s = weight of volume of liquid lifted,

L = wetted length (circumference of ring),

θ = contact angle,

Δx = the distance between the ring and the liquid surface.

The contact angle θ decreases as the extension increases and has the value 0° at the point of maximum force, this means that the term cos θ has the value 1 (WEB_5).

3.5.3. Calculation of Work of Adhesion

Interfacial properties and, in particular the wetting behaviour, play an important role in the wetting of metal–ceramic surfaces. The wetting of ceramic surfaces by liquid is governed by several chemical and physical processes; such as surface free energy (Gibbs free energy) (Contreras et al. 2004).

For determining the surface free energy (ΔG) or W_a are used by measuring the value of γ_{lv} and the contact angle (θ) between the solid and liquid. After measuring these values, the work of adhesion values of uncoated and TiN coated CoCrMo alloys were calculated by the equation 2.6.

CHAPTER 4

RESULTS AND DISCUSSION

This chapter presents the results of characterization of samples by XRD, SEM, EDX, AFM techniques and also wetting analysis. Coated samples were analyzed and compared to uncoated substrates using the above mentioned tools.

4.1. XRD Results

X-ray diffraction (XRD) analysis results of CoCrMo alloy substrates (#29) and TiN coated samples #1 and #7 are shown in Figs. 4.1 and 4.2. Because the coatings were only 3 micrometers thick, the peaks from the substrate material were also observed in the coated samples. In Figs. 4.1 and 4.2, the substrate peaks for γ-(Co, Cr, Mo) and ε-(Co, Cr, Mo) phases were observed. The former phase γ has a face centered cubic (FCC) structure while the latter phase ε has a hexagonal close packed (HCP) structure.

The lattice parameter for the substrate γ-(CoCrMo) phase was calculated for all planes by using the plane spacing equation of cubic structure and the Bragg Equation. The lattice parameter of each phase is indicated in Table 4.1 with the measured and extrapolated *a* and c values. The lattice parameter of the substrate γ-phase was found to be 3.68 Å. The lattice parameters, a and c, for the substrate ε-(CoCrMo) phase was estimated to be 2.54 Å and 4.10 Å, respectively. Based on the intensities of the XRD peaks in Fig.4.1, the volume percent of the substrate γ phase is estimated to be much higher than that of the substrate ε phase (90 % γ phase and 10 % ε phase). The SEM analysis results (section 4.2) indicated that the microstructure for the substrate material (CoCrMo alloy) consists of a fcc matrix with fine hcp platelets (Türkan 2006).

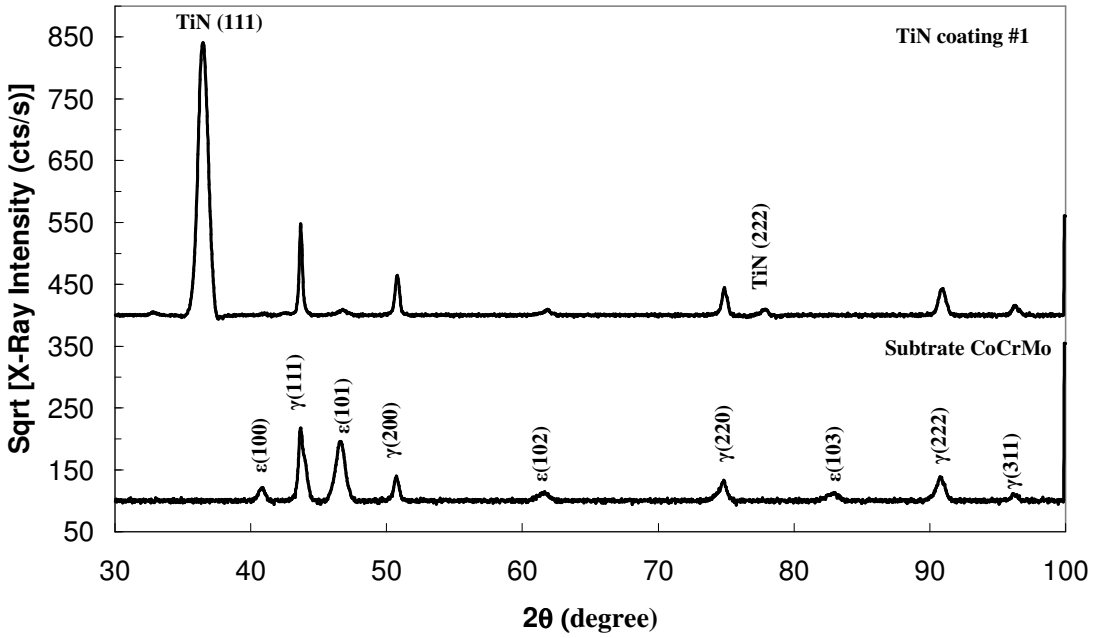

Figure 4.1. XRD patterns of TiN coated (sample #1) and as-polished CoCrMo sample (substrate #29).

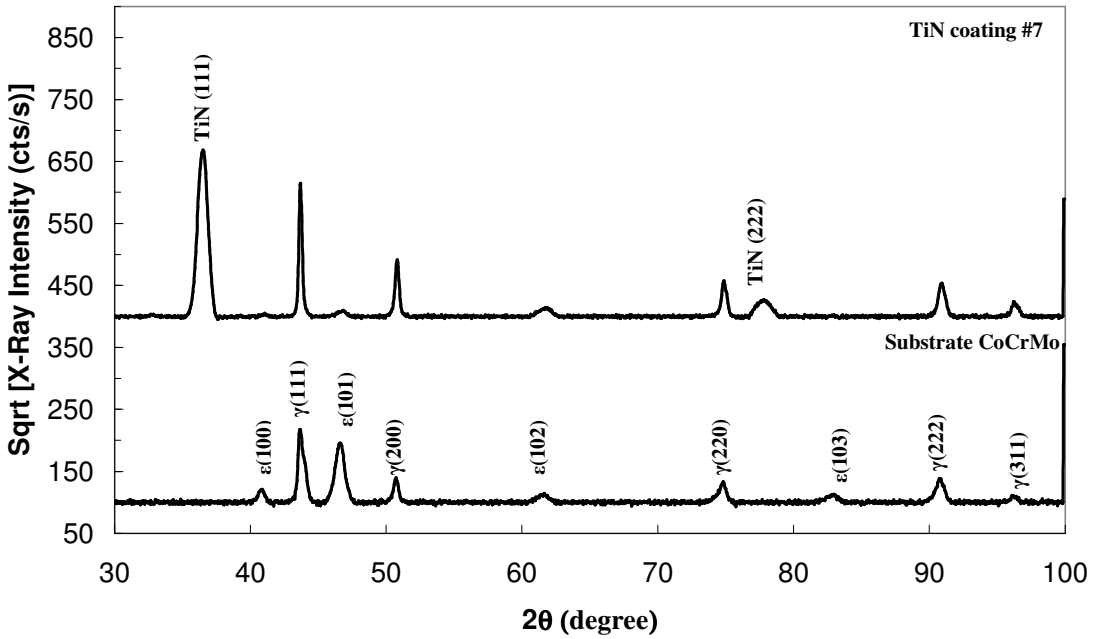

Figure 4.2. XRD patterns of TiN coated (sample #7) and as-polished CoCrMo sample (substrate #29).

Experimental XRD results for the TiN coated specimens (specimens 1 and 7) are also shown in Figs 4.1 and 4.2. As can be seen from these figures, the peaks for TiN are stronger for sample 1 compared to sample 7.

The deposited film was confirmed to be TiN coated CoCrMo with the peak corresponding to the (111) plane being the strongest one. The XRD results show that there are two distinct peaks (at 36.5 and 78 degrees, respectively) associated with TiN phase that is fcc structured. From this XRD spectra, it can be seen that the analyzed TiN film has the main orientation of TiN <111>, besides this, the XRD data indicated some contribution was coming from the substrate phases. This indicates that the x-ray penetration was larger than 3 μm, because the thickness of the TiN film (based on the SEM results) was approximately 3 μm.

The lattice constant, *a*, for the TiN layers (sample #1 and #7) were calculated from the XRD data and were found to be 4.25 Å for both of coated samples (Table 3.1). In the work of Cyster et al., two different TiN coated glass samples (have 1.0 μm and 0.2 μm thicknesses) are investigated. The coating system is reactive sputtering using a DC pulsed magnetron system and has columnar morphology. The lattice constant, *a*, is found 4.24 Å. It has different orientations but the dominant one is (111) plane (Cyster et al. 2002). In another study, which has the similar conditions with the coated samples #1 and #7, the TiN coated S6-5-2 steel with a thickness of approximately 3 μm deposited by PVD is columnar structure. For (111) orientation the lattice parameter, *a*, is found 4.28 Å (Škorić et al. 2004). These differences between the literatures and this study may be occurred due to the differences of the substrate or the coating parameters.

Table 4.1. The lattice parameters of the as-polished sample (#29) and the coated samples (#1 and #7).

Samples	TiN coated CoCrMo		CoCrMo
	#1	#7	#29
FCC phase	a = 4.25 Å	a = 4.25 Å	a = 3.68 Å
HCP phase	—	—	a = 2.54 Å c = 4.10 Å

The (111) which includes the strongest peak was used finding the full width of the diffraction line at half of maximum intensity to determine the grain size. Grain size was calculated by the Debye-Scherrer formula (see equation 3.2). The grain sizes of

TiN layers are about 14 nm for sample #1 and about 11 nm for sample #7. The average value was calculated as approximately 12 nm. There are some differences with the SEM results (based on section 4.2). Cyster et al. is indicated that the grain size of the TiN films increases with increasing film thickness. While the TiN film thicknesses are 0.2 μm and 1.0 μm, the grain sizes are 21 nm. and 25 nm., respectively. The grain size increases by the thickness (Cyster et al. 2002). Another study indicate that for TiN coatings with a thickness of approximately 3 μm deposited by PVD (columnar structure), the grain size is calculated 70 nm but for the (220) orientation (Škorić et al. 2004). However, in our study the coating thickness was 3 μm, the average grain size was 12 nm for the (111) orientation. The differences may be occurred due to have the different thicknesses, different orientation or the different coating parameters. All of the coating conditions influence the grain size of the samples (Zhang et al. 2005).

4.2. SEM Analysis

After XRD characterization technique, the surfaces of the samples were analyzed by using the Scanning Electron Microscopy (SEM) with Secondary Electron mode (SE) and Energy Dispersive analysis of X rays (EDX). Topographic information and chemical compositions of the samples were obtained by means of SEM.

SEM was used for viewing the surfaces in details, also cross-section analysis, which was used for both measuring the thickness of the TiN coated layers and investigating the quality of the coating. The composition of the layers was determined by EDX mode.

4.2.1. SE Analysis

The views of the surfaces, which are substrates (CoCrMo alloys #29 and #44) and TiN coated CoCrMo (#1 and #7) in details are given below parts with obtained images.

4.2.1.1 CoCrMo Alloys

SEM images of two different samples of CoCrMo alloys (as-polished substrate #29 and #44) under the 7 kV accelerating voltage and secondary electron mode are given in Figs. 4.3 and 4.4. As it is seen from the images, there are few differences on the surfaces. The images were taken at different magnitude values. The dissimilarity in the surfaces was obtained more when the magnitude is higher.

In Figs. 4.3 and 4.4, dark regions represent deeper areas whereas brighter represent higher places on the surfaces. The lines are due to the polishing. There are some white points in the surfaces; they can be dust or powder due to cleaning process.

In Fig. 4.3, there are not too many differences in the surfaces, thus, as it is come to Fig. 3.4, there is an efficient dissimilarity observed. This is due to the different conditions. In Fig. 4.4 the magnification was 10000X, whereas, the magnification was 500X for Fig. 4.3. So the more closely to the surface caused more detail observations. In this image, the difference can be occurred the different direction in polishing must be increased number of lines on the surface. Beside these lines, the average roughness (R_a) values also increased (for the #29 and #44 samples, these values were measured as 3.23 nm and 3.62 nm, respectively).

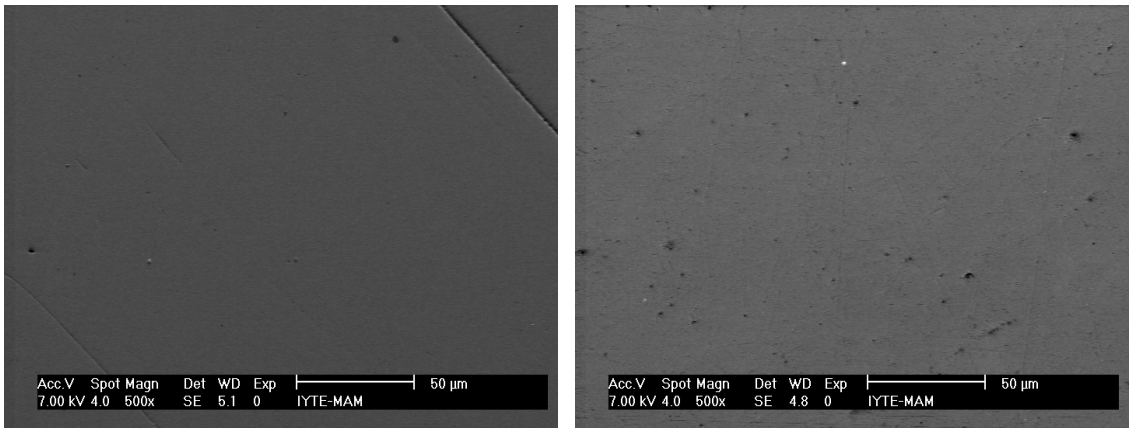

(a) (b)

Figure 4.3. The images of CoCrMo alloys with SE mode with 500X magnification (a) #29 and (b) #44

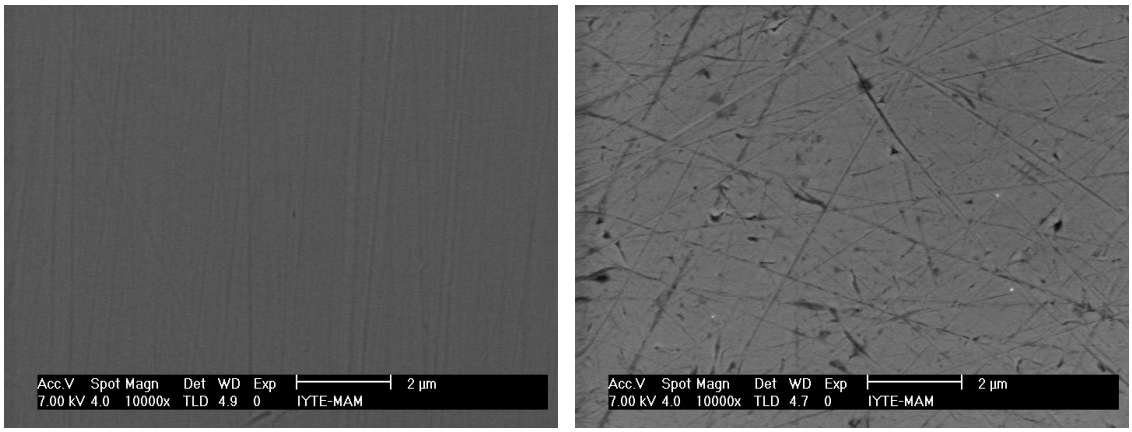

(a) (b)

Figure 4.4. The images of CoCrMo alloys with SE mode with 10000X magnification (a) #29 and (b) #44

4.2.1.2. TiN Coated Specimens

Two different samples of TiN coated substrates (#1 and #7) were investigated by SEM images. The surface morphology of TiN coated specimens under the 7 kV accelerating voltage and secondary electron mode are shown in Figs 4.5, 4.6 and 4.7. These images were taken at 25000X, 150000X and 100000X magnitudes, respectively. The grains are seen more clearly in increased magnifications. Since the columnar growth, which is occurred by PVD coating methods, was used, spaces were occurred and observed around the grain boundaries.

The sample represented as “a” is darker than “b” in figure 4.5. This can be due to SEM’s conditions. Besides grains, there are some dust particles on the surface which are seen white points in the pictures.

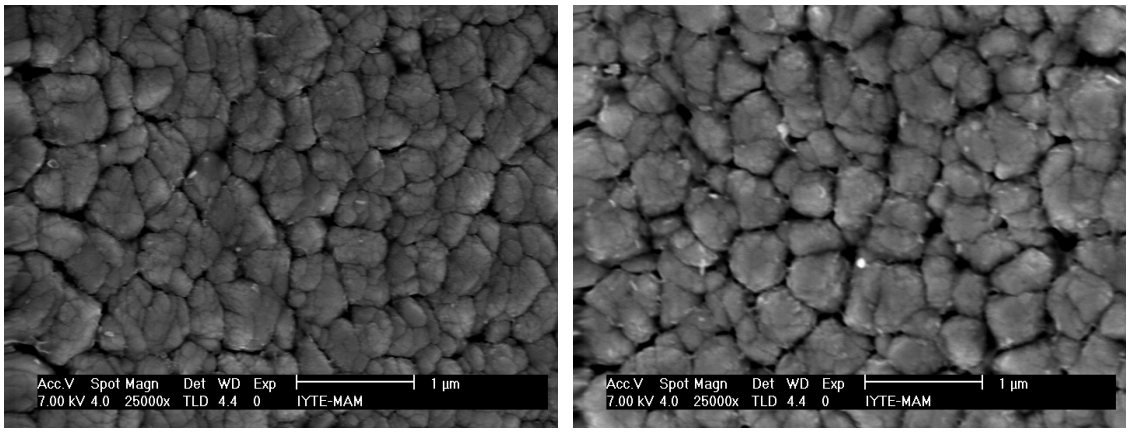

(a) (b)

Figure 4.5. The images of TiN coated CoCrMo alloys with SE mode with 25000X magnification (a) #1 and (b) #7

In Figures 4.6, it is seen that the columns contains pile of grains. While these columns come together, there are some spaces occurred around them; however, more spaces exist on the left one. This may be due to the quality of the coating. It will be observed in detail at the cross-section analysis in the next part.

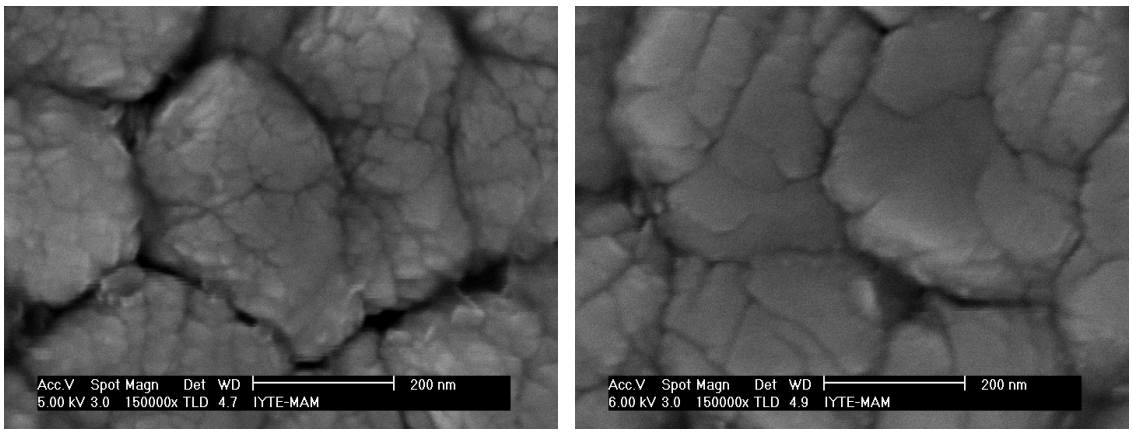

(a) (b)

Figure 4.6. The images of TiN coated CoCrMo alloys with SE mode with 150000X magnification (a) #1 and (b) #7

In Fig. 4.7, the grain size analysis is shown. Firstly, the columns diameter distance was determined by means of SEM. The measurements are given below (Fig. 4.7). The largest diameter value was obtained as 385.19 nm. The least apparent grain

was quantified as 40.41 nm. These values are having an important difference with the grain size calculations in the XRD results (section 4.1). The average value of the grain sizes was found approximately 12 nm, but the apparent grain size is at least 40.41nm. Therefore, the measured part own to piles of grains not grain, they are columns. This measurements indicated that each column consist of lots of grains insides. The other quantifications belong to different part of columns are given below (Fig. 4.7 a and b).

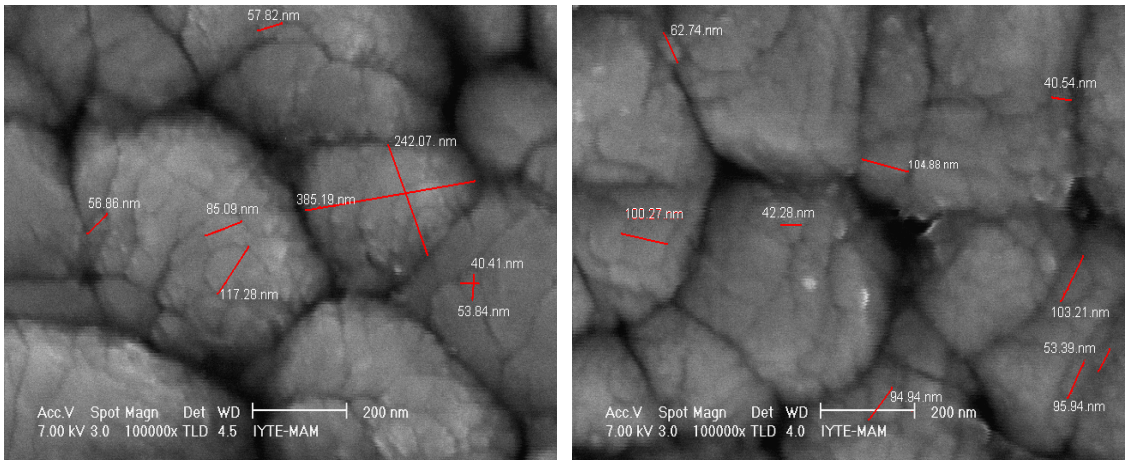

(a) (b)

Figure 4.7. The grain size measurements of TiN coated CoCrMo alloys at the images with SE mode with 100000X magnification (a) #1 and (b) #7

4.2.2. Cross-Sectional Analysis

4.2.2.1. TiN Coated Specimens

Cross-sectional SEM analysis, used for both measuring the thickness and investigating the quality of the film, was done on TiN coated CoCrMo samples. The results are shown in Figs. 4.8 and 4.9. No chemical etching method was used in obtaining the photomicrographs in these figures. The pictures in the figures reveal the TiN deposited layer with a relatively uniform thickness, which effects have an important role on roughness and adhesion treatments. Figs. 4.8 and 4.9 are indicated the TiN film thickness that was obtained as approximately 3 µm. In addition, careful examination of quite a few photomicrographs indicates the growth mode for TiN coating was the columnar type.

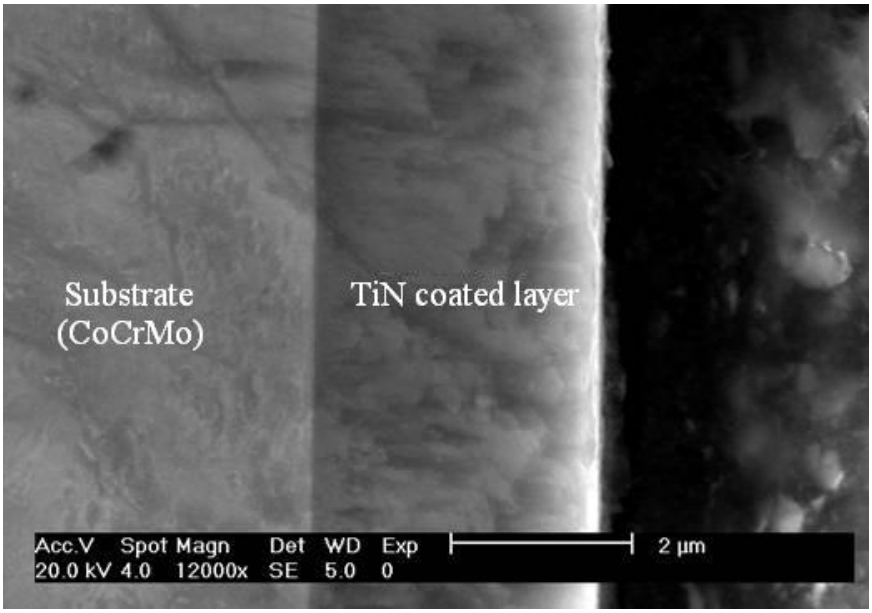

Figure 4.8. Cross sectional SEM data for TiN coated CoCrMo alloys with 2µm in scales with 12000X magnification.

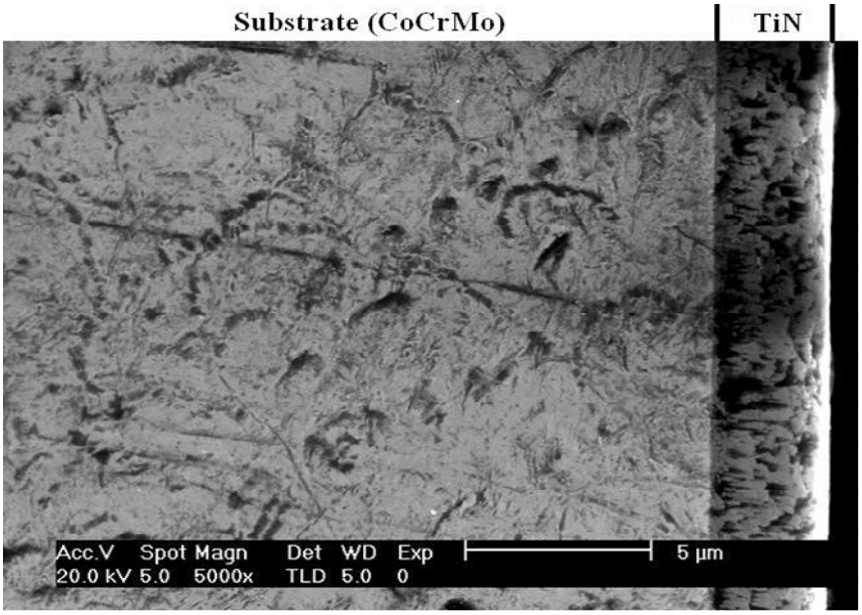

Figure 4.9. Cross sectional SEM data for the TiN coated specimen thickness value in scales 5µm with 5000X magnification.

4.2.3. EDX Analysis

TiN coated samples (#1 and #7) were investigated by the Energy Dispersive analysis of X-rays (EDX) to examine the surface elemental composition. The EDX data shows that besides titanium and nitrogen atoms, oxygen was observed on the surface (Figs 4.10 and 4.11).

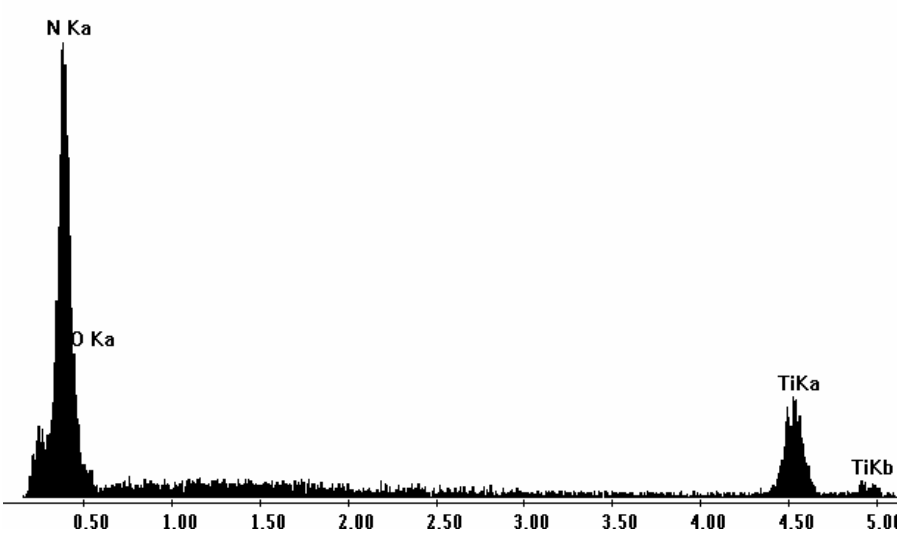

Figure 4.10. The suggested materials with chemical composition in the coated sample #1 according to EDX.

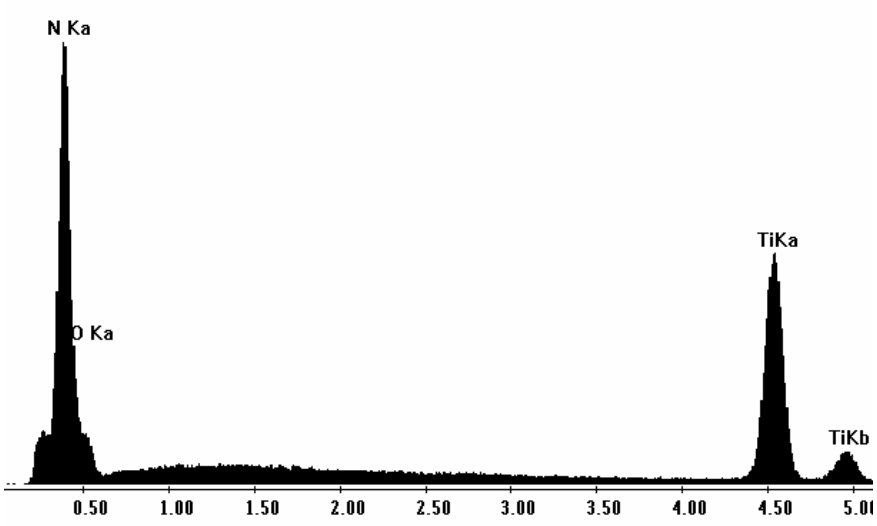

Figure 4.11. The suggested materials with chemical composition in the coated sample #7 according to EDX.

The composition of the films (titanium to nitrogen ratio) was determined by EDX. The EDX analysis results are shown in Table 4.2. As can be seen from this table, Ti/N atomic percentage ratio is not close to 1 (it is about 0.63). For the TiN deposited by PVD composition, an excellent coating is determined by the atomic ratio (Ti/N). It is 1.02 (Škorić et al. 2004). This result (0.63) suggests not a good film stoichiometry. On the other hand, to involve oxygen atom in EDX data, even at small ranges, indicates that there may be an oxide layer on the surface.

Table 4.2. EDX results from TiN coated specimens.

TiN Coating	Elements (at. %)	
	#1	#7
Ti	31,66	34,34
N	50,73	53,6
O	17,61	12,06

The EDX results suggested there is significant difference on the surface. According to the ratio of elements, atomic percent of the nitrogen element was higher than Ti and O elements (Table 4.2). The promising biocompatibility of TiN is attributed to the presence of uniform and homogeneous TiO_2 surface oxide layer. Indeed, the presence of oxygen was obtained from Table 4.2. According to some studies, TiO_2 oxide layer is occurred on the titanium alloys spontaneously. This promotes their good biocompatibility and their excellent resistance to corrosion processes. Fig. 4.12 shows the details of the oxidation process of TiN crystals. After adsorption of molecular oxygen, the TiN surface, which the chemical behaviour strongly depends on their structure and composition, undergoes a reconstruction yielding to the equilibration of the formal oxidation numbers of the surface Ti atoms (Piscanec et al. 2004). In another study, TiN coated glass discs samples, which have two different thicknesses (0,2 and 1 μm, respectively) are used. When they are analyzed by XPS, it indicates the presence of TiN, TiN_xO_y and TiO_2 in similar percentage at surface of both TiN films. A model for the oxidation of TiN has been proposed that on exposure to air TiN oxidizes to 2-3

monolayers of TiO_2. Nitrogen freed as a result of oxidation remains below and any trapped nitrogen combines with TiO_2 to form TiN_xO_y (titanium-oxynitride) (Cyster et al. 2002).

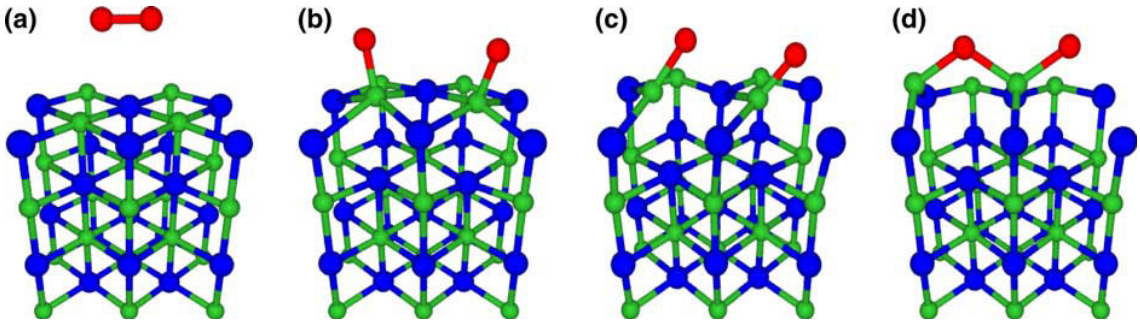

Figure 4.12. Simulation of the adsorption of molecular oxygen on TiN surface (the green ones are Ti, blue ones are N and the red ones are O atoms), in the order (a, b, c and d) how TiO_2 layer is occurred. (Source: Piscanec et al. 2004)

4.3. AFM Analysis

In this section, the surface morphology, the average roughness (R_a) and three-dimensional topology of the substrate and TiN coated samples were obtained. All the samples were scanned at different conditions such as; 30x30 µm (5 times), 50x50 µm (3 times), 100x100 µm (once) with 378 kHz scan rate. In addition to these scans, in 20x20 µm, 10x10 µm and 5x5 µm scales were obtained for TiN coated CoCrMo alloy (sample #8). Roughness analyses were performed to determine the average roughness (R_a). It was obtained and the mean value was calculated for each sample.

Like SEM images, differences in height represented as brightness and darkness in color. AFM images both two and three dimensional for each samples are given below (Figs. 4.13, 4.14, 4.15, 4.16 and 4.17).

AFM images in two and three dimensional of uncoated samples (substrate #29 and #44) are shown in figure 4.13 and 4.14, respectively. It is similar to the SEM image in AFM, there are just polishing lines observed. It is shown that the lines are on the same directions for the sample #29 (Figure 4.13) and on the different directions for the sample #44 (Figure 4.14). There is not much difference between the average roughness

values of the uncoated samples (Table 4.3). This small difference may be occurred the polishing process.

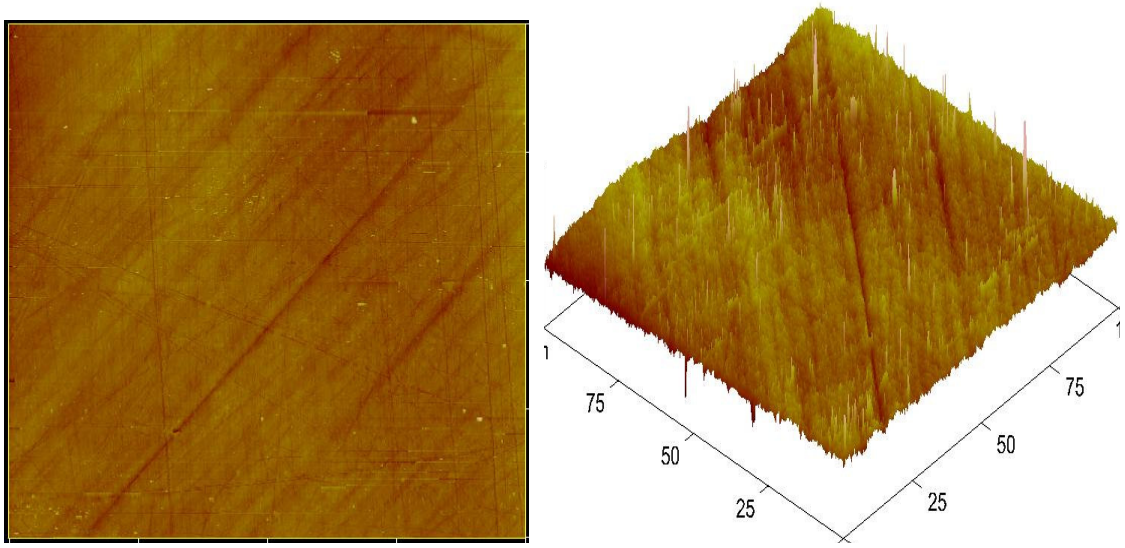

Figure 4.13. For uncoated CoCrMo sample #29, the two and three dimensional morphologies are shown at 100x100 μm conditions. R_a is 4.46 nm.

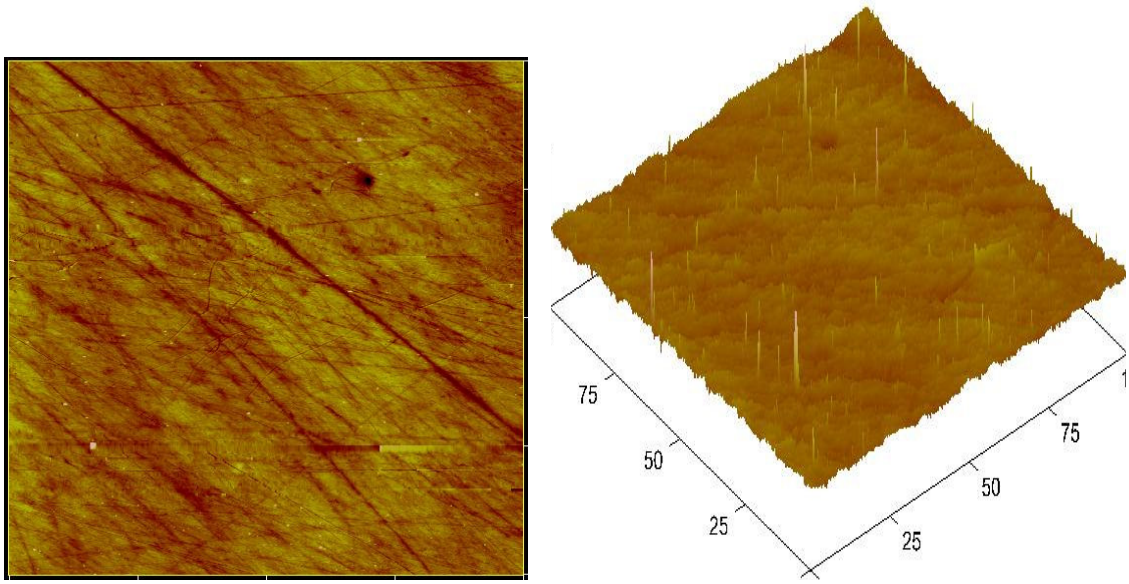

Figure 4.14. For uncoated CoCrMo sample #44, the two and three dimensional morphologies is shown at 100x100 μm conditions. R_a is 3.95 nm.

Two and three dimensional AFM images of TiN coated sample (#8) are shown in Figures 4.15, 4.16 and 4.17. Due to the TiN coated samples (#1 and #7) were so large

to get image in AFM, the coated sample number 8 was used, which was coated in same chamber with the other coated samples. The coating heights, which are the TiN columns, are seen from the three dimensional figures. And the different growth of the columns were influenced the roughness (R_a) values. Although the brighter regions were seen as the grains in two dimensional images, in fact they are columns and each column consists of lots of grains inside. Because, as it measured from Fig. 4.17, the largest grain size was about 340 nm. This value is similar to SEM results (section 4.2.1.2). This means the measured part own to piles of grains not grain from the XRD calculations (section 4.1).

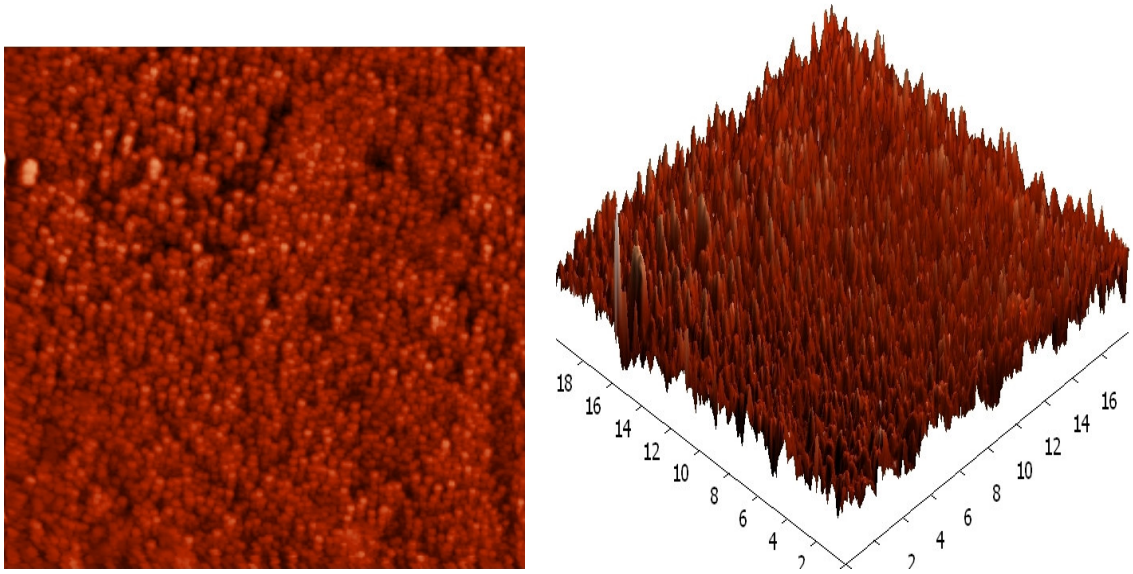

Figure 4.15. For the TiN coated sample, the two and three dimensional morphologies are shown in 20x20 μm scale. R_a is 13.15 nm.

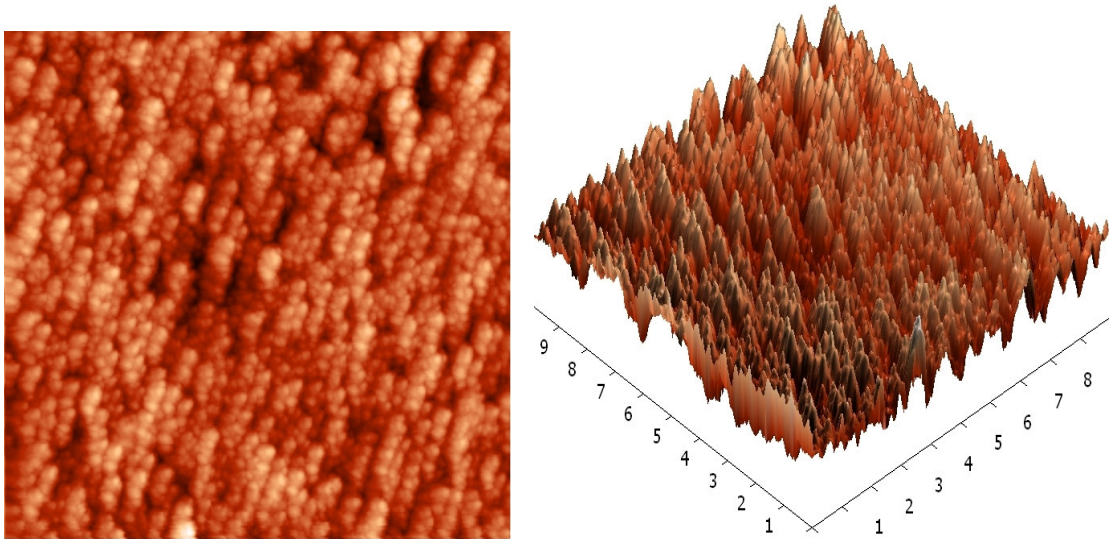

Figure 4.16. For the TiN coated sample, the two and three dimensional morphologies are shown in 10x10 μm scale. R_a is 13.78 nm.

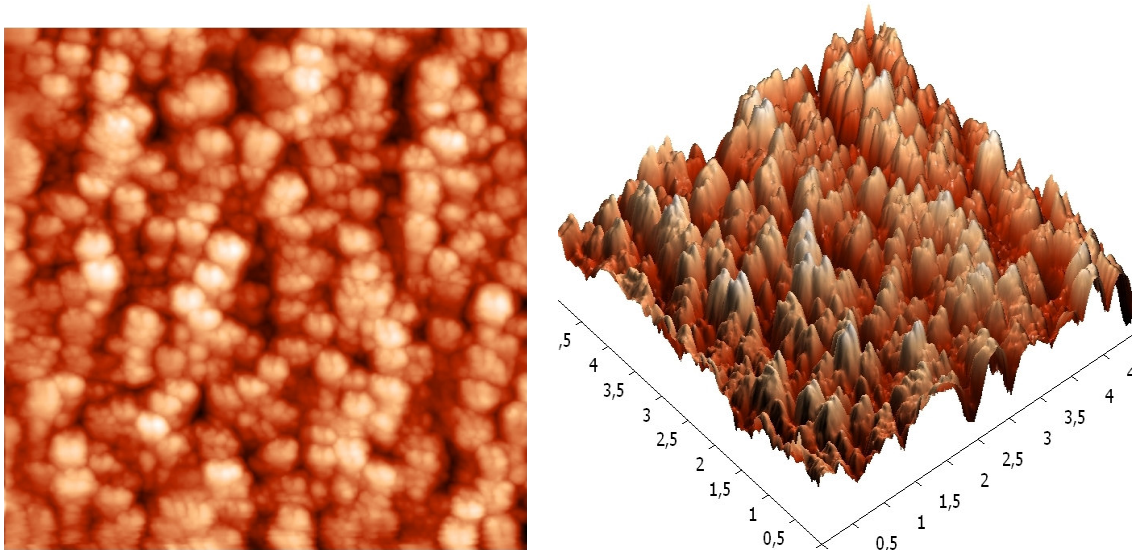

Figure 4.17. For the TiN coated sample, the two and three dimensional morphologies are shown in 5x5 μm scale. R_a is 10.75 nm.

The average roughness (R_a) values of the samples are given in Table 4.3. Three dimensional AFM images and Table 4.3 are also demonstrated that the uncoated surfaces are smoother than the coated surfaces. After coating, the obvious changes on the surface roughness and morphology were obtained. In the study of Tsyganov et al., layers of Ti nitride, Ti oxynitrides TiN_xO_y and Ti oxide are produced by the deposition

on Si at same conditions. The thickness of all layers was about 1 μm and they are fcc structures. When the surface is non-oxide, the roughness is the lowest (Tsyganov et al. 2005). Thus the oxide layer may be occurred on the TiN coated surfaces (section 4.2.2) and this layer may be influenced the roughness. The thickness of the coating also may influence the roughness. In another study, TiN deposited, which is columnar morphology, on glass samples had two different thicknesses, 0.2 μm and 1.0 μm. The roughness values (R_a) increased by the thickness. The average roughness values (R_a) are 1.3 nm and 3.0 nm, respectively. The roughness is increased by the growth of TiN deposited film and film thickness (Cyster et al. 2003). The average thickness of the TiN coated CoCrMo alloys is about 3 μm, so the difference of the roughness values (R_a) can be increased by this thickness value.

Table 4.3. The average roughness (R_a) values of as-polished samples (#29 and #44) and the TiN coated sample (#8).

Samples	R_a (nm)
CoCrMo (as-polished) #29	3.23
CoCrMo (as-polished) #44	3.63
TiN coated CoCrMo #8	12.70

4.4. Wetting Studies

The wetting properties of surfaces (uncoated and coated) were assessed in terms of the change in free energy and the work of adhesion that are calculated from contact angle and interfacial tension values obtained (see section 3.4.3). Basically two test liquids were used as a probe for contact angle measurements and surface free energy calculations: ultrapure water (distilled water) (at 25 ° C and 37 ° C) and simulated body fluid (SBF) at 37 ° C. The effect of coating process on wettability, contact angle was also investigated.

4.4.1. Contact Angle Measurements

As discussed in previous chapter, this is the angle that the tangent to the drop plane makes with the surface plane, in stable equilibrium conditions. Experiments were conducted using the method explained in the material method section. The results are presented as contact angle distributions in Fig. 4.18, 4.19 and 4.20 respectively.

Three types of liquids were used to create a droplet to measure contact angle. These are ultrapure water at 25 ° C, simulated body fluid (SBF) at 37 ° C and ultrapure water at 37 ° C. The mean contact angle values for uncoated (#29 and #44) and TiN coated (#1 and #7) samples were calculated using two hundred measurements for each sample and condition. The mean contact angle values obtained were 74 and 69 degrees for uncoated and coated samples respectively using ultrapure water at 25 ° C (Fig. 4.18). In the figure, the distributions are also regular for the samples. These values were 77° and 73° in the case of simulated body fluid and 85 and 74 degrees in the case of ultrapure water at 37 ° C for uncoated and coated samples respectively (Fig. 4.19 and 4.20). The distributions of the graphs in these figures are regular for all samples, but for coated samples it is larger than uncoated samples. The distribution differences in the figures can be due to the coating properties such as the different column lengths or the oxidation.

The mean values of the contact angles and the standard deviation were calculated and they are shown in Table 4.4. The mean and the standard deviation could be used to present the distribution of contact angles on the solid surfaces. The standard deviation provides valuable information regarding heterogeneity of the surface. So the table indicates that the TiN coated samples may be more heterogeneity, but they are more hydrophilic.

For uncoated and coated samples, the contact angle results by using SBF and ultrapure water at 37 ° C clearly show the influence of temperature on contact angle. This is most probably due to the cohesion energy known as the energy per molecule inside the liquid. Good wetting means that the interfacial bond is energetically nearly as strong as the cohesion bond of the liquid itself (Eustathopulos et al. 1999 and Contreras et al. 2004). While increasing in temperature causes expending in hydrophobic behavior which is related with increasing contact angle (Zettlemoyer 1960, Melrose 1968 and Borruto et al. 1998).

Table 4.4. Contact angle values of as-polished samples (#29 and #44) and coated samples (#1 and #7) by ultrapure water and SBF at the different temperatures.

Samples	$\theta_{mean} \pm \Delta\theta$ (degree)		
	Ultrapure water (25 ° C)	Ultrapure water (37 ° C)	Simulated Body Fluid (37 ° C)
Uncoated #29	75 ± 3	85 ± 1	78 ± 2
Uncoated #44	72 ± 2	84 ± 1	75 ± 2
Uncoated (Mean)	74 ± 3	85 ± 1	77 ± 2
TiN coated #1	68 ± 2	73 ± 2	72 ± 3
TiN coated #7	69 ± 3	74 ± 3	73 ± 3
Coated (Mean)	69 ± 3	74 ± 3	73 ± 3

Table 4.4 gives the contact angle values for coated and uncoated samples for different liquid types. It is seen that TiN coated samples always have lower contact angle values than uncoated ones. This difference was the largest in case of ultrapure water at 37 ° C. This shows the significance of the effect of temperature. In case of simulated body fluid contact angle values get lower again even though the temperature is 37 ° C. This might be due to the presence of some ions in the system.

To explain the difference between coated and uncoated samples obtained surface roughness was also measured. Because it is known that surface roughness effects contact angle (Adamson, 1989). This relation, however, is complex will be discussed in the next section in detail roughness of surfaces were found to be 3.43 nm and 12.70 nm for uncoated and TiN coated samples, respectively. If one thinks about the size of liquid droplets used to measure contact angles in this study, this much roughness may be safely assumed to be negligible. The drops are almost 5 mm in size. Therefore this difference in the contact angle is due to the chemistry of surfaces, not because of roughness degrees.

A common value of a water contact angle for TiN layer is about 68° in literature, which measured contact angle by sessile drop methods on a TiN-PVD layer with

distilled water in the same drop size (Lugscheider et al. 2003). This value has the similarity with the contact angles of the TiN coated samples, so the existent data has the good agreement with the literature inputs.

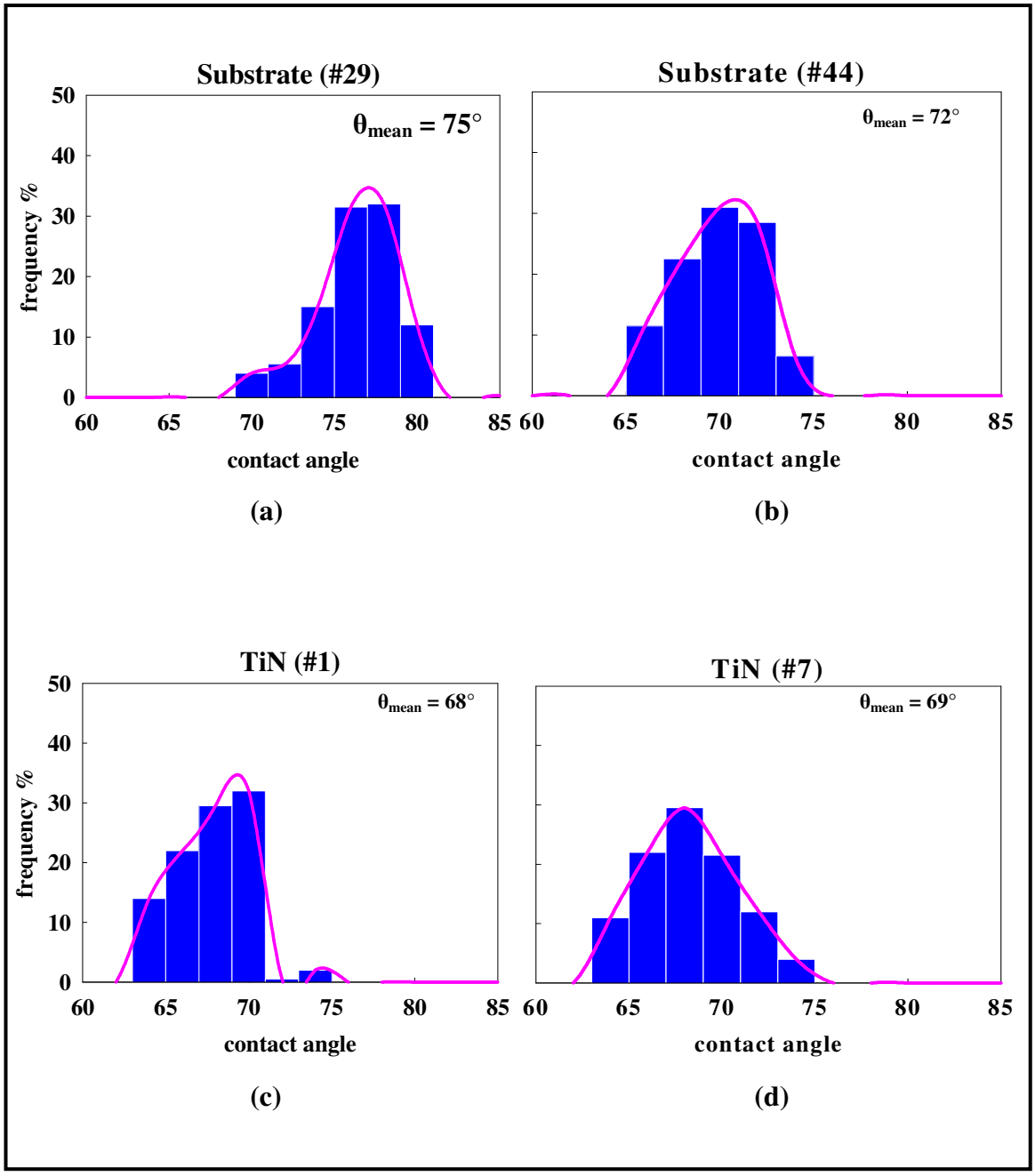

Figure 4.18. Frequency percents of contact angles by ultrapure water at 25°C (a) CoCrMo #29 (b) CoCrMo #44 (c) TiN coated CoCrMo #1 (d) TiN coated CoCrMo #7

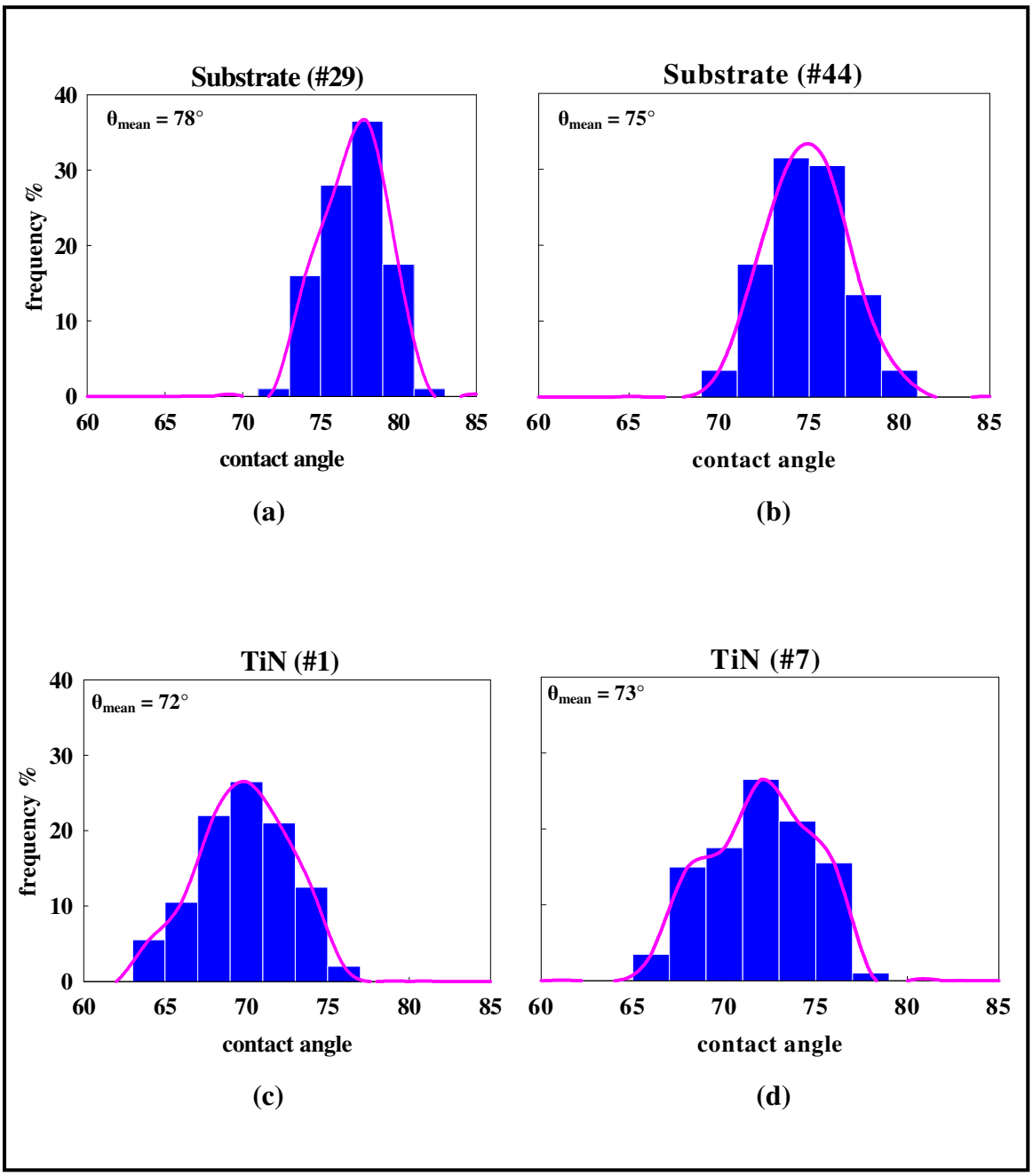

Figure 4.19. Frequency percents of contact angles by simulated body fluid at 37°C (a) CoCrMo #29 (b) CoCrMo #44 (c) TiN coated CoCrMo #1 (d) TiN coated CoCrMo #7

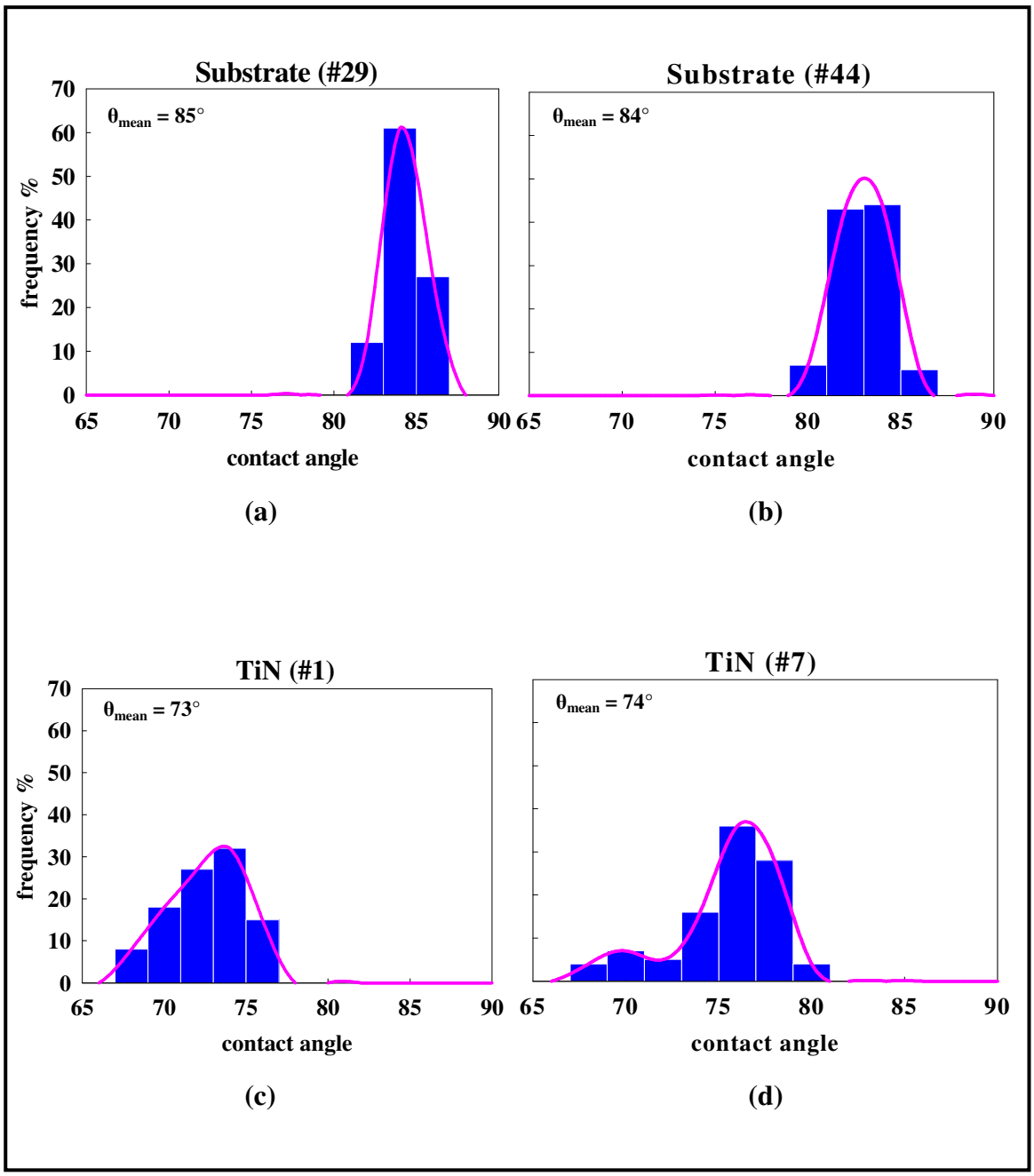

Figure 4.20. Frequency percents of contact angles by ultrapure water at 37°C (a) CoCrMo #29 (b) CoCrMo #44 (c) TiN coated CoCrMo #1 (d) TiN coated CoCrMo #7

4.4.2. Roughness Effect

It is known that the changes in surface roughness, surface oxygen content (see section 4.2.2) and surface energy (see section 4.4.3) generated by the coating treatment could be the factor influencing the wettability characteristics of the biomaterials (Hao et al. 2005). From Table 4.4, the differences between the contact angle values of the samples can be related with the roughness, so the connection was investigated. An uncoated sample (#44) roughed with three kinds of sandpaper having various grit sizes. They were 2500, 1000 and 320, whose roughness values increase respectively. After polishing, the contact angles were measured using the sessile drop technique by ultrapure water at 25 ° C. The drop sizes were about 60 μL. The contact angle values for the different roughness values were obtained from fifty measurements and then the average and the standard deviation was calculated for each roughness value.

The average roughness (R_a) and the contact angle values are shown with their standard deviations in Table 4.5. From Table, it can be obtained the contact angle values are influenced by the roughness. The contact angle values decreased when the average roughness increased. The standard deviation also changed by the roughness. While the roughness increased, the standard deviation increased due to the rising the surface heterogeneity.

There is a contradiction in terms of relationship between the roughness and contact angle in the literature. According to Adamson 1967 and Feng et al. 1998, the contact angle is observed on Ti surface by pure distilled water (the drops are ≈ 1-2 mm in diameter). Ti surface has various degrees of surface roughness produced by mechanical polishing and the contact angle values are approximately inversely proportional to the surface roughness values (Feng et al. 1998). They are indicated that if contact angle (θ) is less than 90°, θ is decreased by roughness, while if θ is greater than 90°, it is increased by roughness. Table 4.5 shows that when the roughness values increase, the contact angle decrease. Due to reason that all contact angle values were observed less than 90°, it can be said the contact angle decreases with increasing roughness.

Table 4.5. Average roughness values and the measured contact angle values of as-polished sample (#44) by using ultrapure water (25 ° C)

AVERAGE ROUGHNESS (nm)	CONTACT ANGLE (degree)
Ra (mean) = 13 ± 2	$\theta_{mean} = 65° \pm 3$
Ra (mean) = 61 ± 8	$\theta_{mean} = 62° \pm 2$
Ra (mean) = 100 ± 23	$\theta_{mean} = 58° \pm 3$

However, the roughest surface has the highest water contact angle, according to (Ponsonnet et al. 2003). The water contact angle measurements by sessile methods were performed directly on rough NiTi samples (NiTi 80, 400 and 2400). The order of magnitude of the water contact angles is as a function of roughness. The angles ranging get from 45° to 75° and roughness from 0.3 to 3 μm, respectively. These results have a contradiction with Table 4.5. This dissimilarity can be observed due to the using different samples or the chemical interactions between water and the samples.

In this study, the water drop is about 5 mm in diameter and the average roughness value is a few nanometers, so the size can not be discussed well in detail. Thus, the shape of the water drop is so large on such rough surfaces. It can not give correct values between the roughness and the surface hydrophobicity.

4.4.3. Surface Tension Measurements

Interfacial (surface) tensions of ultrapure water and the simulated body fluid (SBF) at different temperatures were measured and presented in Table 4.6. Each measurement was done almost twenty times and the average values were tabulated in Table 4.6. The surface tension of ultrapure water at 25 ° C was measured as 71 $mN.m^{-1}$, that is in agreement with literature value (72 $mN.m^{-1}$) (Lugscheider et al. 2003). This value decreased to 63 $mN.m^{-1}$ when temperature increased to 37 ° C. According to Keesom interaction of the dipoles (permanent dipole/permanent dipole interaction), the dipole interaction strength is inversely proportional to the temperature therefore all

other things being equal an increase in the temperature should result in a decrease in the dipole attraction which in turn should lead to decrease in surface tension.

Another reason is that to increase temperature causes increasing in cohesion energy known as the energy per molecule inside the liquid. The surface tension is $\gamma \approx U / 2\pi a^2$ (see section 2.3); a^2 is the exposed area of a molecule (WEB_4). Then, when the temperature is higher, the a increases so surface tension is lower.

Table 4.6. The average values of surface tension of Ultrapure Water (25 ° C), Ultrapure Water (37 ° C) and Simulated Body Fluid (37 ° C)

ULTRAPURE WATER (25 ° C) ($mN.m^{-1}$)	ULTRAPURE WATER (37 ° C) ($mN.m^{-1}$)	SBF (Simulated Body Fluid) (37 ° C) ($mN.m^{-1}$)
71 ± 0,3	63 ± 2,8	62 ± 6,1

In vivo the environment is aggressive both ionic and cool. Then the simulated body fluid value is the close to the body environment. In spite of it is known (Adamson 1967) the surface tension increase by the ion concentration, it can be seen Table 4.6, there is not much difference between ultrapure water and simulated body fluid in the same temperature. It may be occurred by buffer, due to the presence of buffer in SBF, which without strong buffers do not mimic the homeostasy of human plasma, plays an inhibiting role in the mineralization process (Marques et al. 2003). And also SBF and ultrapure water have close pH, which are 7.4 and 7, respectively. The mean surface tension value for SBF was obtained about 62 $mN.m^{-1}$ (Table 4.6) and this value is approximately 60 $mN.m^{-1}$ in the work of (Marques et al. 2003) by the same range of ion consideration.

4.4.4. Work of Adhesion and Change of Gibbs Free Energy

To determine the wetting properties of surfaces, work of adhesion and the Gibbs free energy change were calculated using contact angle and surface tension values obtained before. The work of adhesion is the reversible work required to separate unit area of liquid from the substrate. In contrast, the change in Gibbs free energy (ΔG) is

the spreading energy when the drop falls on the substrate spontaneously. In systems, as W_a quantity gets more and also ΔG quantity gets low, the determination of wettability and adhesion get more. In other words, the change in Gibbs free energy and work of adhesion has an inverse relation with each other (section 2.4).

Equation 2.6 was used to calculate work of adhesion for each sample and they are given in Table 4.7. That is, ΔG is equal to - W_a. The work of adhesion values of TiN coating on CoCrMo samples are higher than as-polished CoCrMo alloys. It means that the wettability is enhanced by coating.

The calculated work of adhesion / Gibbs free energy change values were given in Table 4.7. It is seen that these values are higher in case of coated samples for all the cases. The highest work of adhesion was obtained in case of coated sample in ultrapure water at 25 °C. Increasing temperature and using simulated body fluid decreases work of adhesion. That is wetting of these samples in ultrapure water will be more spontaneous compare to the simulated body fluid. However, ultrapure water becomes similar to the simulated body fluid at 37 ° C. Lugscheider et al. 2003 have been also calculated the work of adhesion as 98.97 $mJ.m^{-2}$ for TiN using the contact angle value as 68 degree. This is also in good agreement with the values of this study.

Table 4.7. Work of adhesion values for as-polished samples (#29 and #44) and coated samples (#1 and #7) by ultrapure water and SBF at the different temperatures.

Samples	W_a ($mJ.m^{-2}$) = - ΔG		
	Ultrapure water (25 ° C)	Ultrapure water (37 ° C)	Simulated Body Fluid (37 ° C)
Uncoated #29	89.38	68.49	74.89
Uncoated #44	92.94	69.59	78.05
TiN coated #1	97.60	81.42	81.16
TiN coated #7	96.44	80.37	80.13

The work of adhesion values of uncoated sample (CoCrMo) are in agreement with the literature values (Gispert et al. 2006). In their study Hank's balanced salt

solution (HBSS) and HBSS+BSA (bovine serum albumin) were used. Their surface tension values are the same with ultrapure water (71 $mN.m^{-1}$) and simulated body fluid (62 $mN.m^{-1}$), respectively. For CoCrMo in HBSS (25 ° C) W_a is 94 $mJ.m^{-2}$ and in HBSS+BSA W_a is 77 $mJ.m^{-2}$, which are in good agreement with the values of this study (Table 4.7).

The work of adhesion determines the wetting characteristics but another important factor in the wetting is the surface energy of the solid. A significant increase in total solid surface energy enhances the wetting. Especially the increase in polar component of total solid surface energy (γ_s^p) has a positive effect upon the action of wetting and adhesion. In (Hao et al. 2005) study, the exhibited increase in the surface energy, in particular polar nature of the stainless steel after CO_2 laser treatment, generated the higher wettability characteristics such as the lowest θ with physiological test liquids. In Table 3.7 the differences between W_a of coated and uncoated samples can be obtained due to this affect. The coating can cause the increasing the solid surface tension (especially the polar part), so the adhesion and hydrophilicity (Table 4.4) values are higher.

The surface oxygen content also influences the wettability characteristics of surfaces. In the study of Feng et al. 1998 the relationship between oxide layer and contact angle was investigated for Ti surfaces. It was found that the water drop spreads better on well-polished Ti surface in air than in non-oxygen environment. That is, when surface is in air environment, the contact angle of Ti surface decreased. It was said that an oxide layer has developed on Ti surface and this layer made the surface more hydrophilic. As a result, the hydrophilicity increases with oxidation. The TiN coating is generally assumed to be covered by an oxide layer. It was discussed in section 4.2.2, so the differences in W_a values between coated and uncoated samples (Table 4.7) can be due to the presence of oxide layers.

In the literature, stronger bone tissue reactions to implants with a thick oxide layer were indicated and the best thicknesses were between 600 and 1000 nm. (Nishiguchi et al. 1999, Sul et al. 2002, Garcia-Alonso et al. 2003 and Spriano et al. 2005). While CoCrMo alloys have a few nanometers oxide layers (section 1.1), the thickness of TiN was estimated at least a few nm according to Logothetidis et al. 1999. In other words, TiN has more oxide layers than CoCrMo alloys, so it can be more hydrophilic.

Due to the oxide layer, it was observed a significant bioactivity of TiN-coated samples according to (Piscanec et al. 2004). It was indicated that it was observed a calcium phosphate aggregation at the interface between (oxidized) TiN and physiological fluid. The oxidized TiN surface can promote the deposition of calcium phosphate from the body fluid. This spontaneous nucleation of calcium phosphates on oxidized TiN surface enhances the osteointegration.

The working conditions of human implants have different properties. Firstly, the implants must be designed to long-lasting operation by very low wear rates. For Co–Cr–Mo alloys, the wear resistance is good enough but the surface modification is come well by decreasing the friction, then further extension of expected lifetime (Jagielski et al. 2006). The presence of oxygen promotes the good biocompatibility and the excellent resistance to corrosion processes and friction, which provide the biomaterials the long-term subjects. It is known that TiN is obtained a good corrosion resistance and also it has the low friction coefficient (Amadeh et al. 2001 and Jagielski et al. 2006). So when the CoCrMo alloy is coated by TiN layer, it has an excellent wear and friction factor for a biomaterial.

Secondly, the mechanical implants take place in the synovial fluids (body fluid). The presence of the body fluid in the contact area has an excellent condition for correct operation of hip joints and their prostheses. Wettability is important for good cell adhesion, contact with the body tissue and lubrication of the contact area. The changing of surface wettability is important characteristic for cell adhesion and friction properties. A good lubrication and reduced friction coefficient of the whole implant system should be ensured the modification of both metallic (or ceramic) and polymer parts of the prosthesis aiming the formation of hydrophobic/hydrophilic system (Jagielski et al. 2006).

It was tested using five materials two types of couplings (hydrophilic-hydrophilic, hydrophobic-hydrophobic, and hydrophilic-hydrophobic) by using distilled water in the study of (Borruto et al. 1998). In the end of the test, very hydrophobic and very hydrophilic couplings have a positive effect on the system for the friction aspect. According to Borruto et al., when the contact angle value is in between $45° \leq \theta \leq 90°$, the system is basically hydrophobic. In our study, TiN coated samples (69°) and CoCrMo alloy samples (74°) are basically hydrophobic. And also the ultra high molecular weight polyethylene (UHMWPE), which the femoral head (TiN coated or as-polished CoCrMo alloys) inserts into, is the basically hydrophobic (56°) (Urkac 2006).

That is, in this study hydrophobic-hydrophobic coupling was constructed. This coupling can be a good replacement for different areas in vivo (especially total hip replacements), in spite of the best coupling is hydrophilic-hydrophobic.

The relationship between friction and work of adhesion related with the surfaces of the tribological pairs depends on the lubrication system. In general, a high value for the work of adhesion implies a strong friction in the hydrodynamic lubrication regime, while the opposite is true for boundary lubrication (Hall et al. 1997 and Gispert et al. 2006). In this study, the coated samples have higher work of adhesion values than the uncoated samples. So the friction is high for TiN coated samples than CoCrMo alloys in the hydrodynamic lubrication regime. However, the TiN coated CoCrMo surface is not highly hydrophilic, so the friction rate is not much. The values of W_a for TiN coated samples are high enough for hip joint replacements (Lugscheider et al. 2003 and Gispert et al. 2006).

Finally, the deposited layers are reduced the risk of accidental failure of the implant. The hip joint prostheses made of titanium alloy: carbon and nitrogen implantation into their femoral heads resulted in order-of-magnitude reduction of wear (Sioshansi et al. 1996), whereas the contact with the bone of the stem part can be improved by oxygen implantation (Mandl et al. 2003 and Jagielski et al. 2006). From this approach, TiN coated CoCrMo alloys (without oxidation) are appropriate for femoral head to prevent the ion releasing in order to reduce the wear. In addition, TiN coated CoCrMo alloys, which have an oxide layer, are suited to the stems in bones in terms of the bioactivity (bone compatibility).

CHAPTER 5

SUMMARY AND CONCLUSION

Wettability, defined as the ability of any solid surface to be wetted when in contact with a liquid, is one of the most important properties of biomaterials since highly wettable (hydrophilic) surfaces are expected to disclose better adhesion of the cells. Also, it is known that the wettability of the prosthetic materials affects friction and wear. The wettability characteristics of a biomaterial's surface can be improved by surface modification techniques.

In this study, wettability characteristics of TiN coated CoCrMo orthopedic alloy materials were investigated. Physical vapour deposition (PVD) method at 550 ºC for 6 h was used to deposit titanium nitride (TiN) on CoCrMo alloy substrates. Totally, 8 CoCrMo alloy specimens were coated with TiN, but in this study, only three of them were investigated. Also, as the substrate alloys, two CoCrMo alloy samples were researched.

The TiN coated layer microstructures, roughnesses, thicknesses, and elemental composition were investigated by XRD, AFM, and SEM (in both SE and EDX modes) was used to investigate the TiN coated CoCrMo alloys. Wetting studies involved contact angle and surface tension (surface energy) measurements using ultra pure water and simulated body fluid (SBF) as test liquids at 25 °C and 37 °C. The contact angles of the TiN coated and uncoated (polished) CoCrMo alloy materials were studied by the sessile drop method using a contact angle analyzer and the surface tension of the test liquids was measured by the ring method using a digital tensiometer.

The XRD results indicate that the fcc TiN coatings exhibited (111) preferred orientation while the SEM analysis indicated quite uniform TiN coated layers (about ~ 3 μm thick) with a columnar growth mode. Based on the AFM results, the average roughness (Ra) value for the uncoated (polished) CoCrMo alloy surface was found to be ~ 3 nm, while the TiN coated surfaces had roughness values ranging from ~ 11 to 14 nm.

The wetting analysis results show that the TiN coated layer has better wettability characteristics compared to the uncoted (polished) CoCrMo substrate alloy. The contact angle measurements show that the contact angle values for the TiN coated samples are

lower than the uncoated samples for all liquid types. Based on the measured contact angle and surface tension values, to determine the wetting properties for biomaterials, the work of adhesion (the change in the Gibbs free energy) values were calculated. Due to the work of adhesion (W_a) was found high enough for better adhesion and ΔG was found negative ($\Delta G = - W_a$) for the spreading of the drop gets spontaneously. The findings suggest the TiN coated layers have better adhesion ability compared to the uncoated CoCrMo alloy. In other words, the TiN coated CoCrMo alloy has a lower adhesion resistance compared to the uncoated CoCrMo alloy.

The lower contact angles (lower adhesion resistance) for the TiN coated samples were attributed mainly to the rougher surfaces associated with the coated surfaces in comparison with the relatively smooth surface of the uncoated sample. The roughness effect was verified by contact angle measurements on the CoCrMo substrate materials that had been polished to various degrees of roughnesses. These measurements clearly showed that the rougher the substrate surfaces are the lower the contact angle values.

Lower adhesion resistance (or better adhesion ability) of the TiN coated layers compared to the uncoated ones was also explained by the surface oxygen content and the surface oxide layer on the TiN coated CoCrMo alloy. The EDX analysis results indicated significant amount of oxygen (ranging from ~ 12 to 18 at. %) on the surface of the TiN coated layers suggesting the formation of a possible oxide layer (TiO_2) on the TiN coated layer. It is discussed that the oxide layer may make the coated surface more hydrophilic. It was also argued that the better wettability characteristics of the TiN coated surfaces may be due to a possible increase in the surface energy of the coated surfaces compared to the uncoated surfaces.

The experimental findings in this research show that the TiN coated samples have more hydrophilic properties than the uncoated samples. This is believed to be an advantage for the biomaterials in terms of the osteointegration (the deposition of calcium phosphate). It means that it is a chemical adsorption between the TiN layer and the body fluid circulating in the bone. The oxide layer enhances the chemical adsorption on TiN surface. Because of this, W_a gets higher, when the oxide layer is present.

In conclusion, to prevent friction and the release of metal ions from CoCrMo orthopedic implant materials into body tissue, TiN layer is applied. It is an effective barrier to ion release and also has a less friction rate. These TiN coated CoCrMo alloys are the offered possibilities for the hip joint prostheses. For CoCrMo alloys the wear resistance is good enough but the surface modification focuses on friction reduction.

The mechanical contact takes place in the synovial fluids for the natural hip joints and their prostheses. The presence of the body fluid in the contact area appears as a mandatory condition. Controllability of the wetting is important for cell adhesion, contact with the body tissue and lubricant of the contact area. The surface wettability is particularly specific characteristic of the method critical for cell adhesion and friction properties. Due to encouraging friction by high work of adhesion, while the cell adhesion must be high in the contact with the bone of the stem part to get the adsorption better, it must be low to protect the articulating surface for the femoral heads of the hip joints. When the stem part has high surface oxide content, the adsorption can get better. However, for the femoral heads it can be better that the oxide content rates of TiN surfaces are low.

In the future, to investigate the thickness of the oxide layer on the surface x-ray photoelectron spectroscopy (XPS) analysis can be studied. Also, to get more investigation can be done; including examination by using cell, organ cultures and then tests will be based on implantation in animal organisms.

REFERENCES

Adamson A.W., 1967. “Physical Chemistry of Surfaces”, Interscience Publishers, pp. 357-359

Agathopoulos S., Nikolopoulos P., 1995. “Determination of the energy of the interactions between oxides and biological liquids”, Fourth Euro ceramics, Vol. 8, pp. 319–24

Amadeh A., Heshmati-Manesh S., Labbe J.C., Laimeche A., Quintard P., 2001. “Wettability and corrosion of TiN, TiN±BN and TiN-AlN by liquid steel”, Journal of the European Ceramic Society, Vol. 21, pp. 277-282

Amaral M., Lopes M.A., Santos J.D., Silvaa R.F., 2002. “Wettability and surface charge of Si3N4–bioglass composites in contact with simulated physiological liquids”, Biomaterials, Vol. 23, pp. 4123-4129

Annarelli C.C., Fornazero J., Cohen R., Bert J., Besse J.-L., 1999. “Colloidal protein solutions as a new standard sensor for adhesive wettability measurements”, Journal of Colloid Interface Science, Vol. 213, pp. 386-394

Azevedo A.F., Corat E.J., Ferreira N.G., Trava-Airoldi V.J., 2005. “Wettability and corrosion tests of diamond films grown on Ti6Al4V alloy”, Surface & Coating Technology, Vol. 194, pp. 271-275

Borruto A., Crivellone G., Marani F., 1998. “Influence of surface wettability on friction and wear tests”, Wear, Vol. 222, pp. 57-65

Chenglong L., Dazhi Y., Guoqiang L., Min Q., 2005. “Corrosion resistance and hemocompatibility of multilayered Ti/TiN-coated surgical AISI 316L stainless steel”, Materials Letters, Vol. 59, pp. 3813-3819

Contreras A., Bedolla E., Pérez R., 2004. “Interfacial phenomena in wettability of TiC by Al–Mg alloys”, Acta Materialia, Vol. 52, pp. 985–994

Cullity B.D., 1978. “Elements of X-ray Diffraction”, Addison Wesley Publishing Company, pp. 292-295

Cyster L.A., Grant D.M., Parker K.G., Parker T.L., 2002. “The effect of surface chemistry and structure of titanium nitrade (TiN) films on primary hippocampal cells”, Biomolecular Engineering, Vol. 19, pp. 171-175

Cyster L.A., Parker K.G., Parker T.L., Grant D.M., 2003. “The effect of surface chemistry and nanotopography of titanium nitrade (TiN) films on 3T3-L1 fibroblasts”, Wiley Periodicals, Inc. J Biomed Mater Res, Vol. 67A, pp. 138-147

Davidson J.A., 1993. “Characteristics of metal and ceramic total hip bearing surfaces and their effect on long-term ultra high molecular weight polyethylene wear”, Clinic. Orthop. Rel. Res., Vol. 294, pp. 361-378

Duisabeau L., Combrade P., Forest B., 2004. “Environmental effect on fretting of metallic materials for orthopaedic implnts”, Wear, Vol. 256, pp. 805-816

Ensinger W., 1998. “Ion bombardment effects during deposition of nitride and metal films”, Surface and Coatings Technology, Vol. 99, pp. 1-13

Eustathopoulos N., Nicholas M.G., Brevet B., Cahn R.W., 1999. “Wettability at high temperatures”, Pergamon Materials Series, Vol. 3, pp. 45

Feng A., McCoy B.J., Munir Z.A., Cagliostro D., 1998. “Wettability of transition metal oxide surfaces”, Materials Science and Engineering, Vol. A242, pp. 50-56

García-Alonso M.C., Saldaña L., Vallés G., González-Carraco J.L., 2003. “In vitro corrosion behaviour and osteoblast response of thermally oxidized Ti6Al4V alloy”, Biomaterials, Vol. 24, pp. 19-26

Gispert M.P., Serro A.P., Colaço R., Saramago B., 2006. “Friction and wear mechanisms in hip prosthesis: Comparison of joint materials behaviour in several lubricants”, Wear, Vol. 260, pp. 149-158

Hall R.M., Unsworth A., 1997. “Friction in hip prosthesis”, Biomaterials, Vol. 18, pp. 1017-1026

Hao L., Lawrence J., 2006. “Effects of Nd: YAG laser treatment on the wettability characteristics of a zirconia-based bioceramic”, Optics and Lasers in Engineering, Vol. 44, pp. 803-814

Hao L., Lawrence J., Li L., 2005. “The wettability modification of bio-grade stainless steel in contact with simulated physiological liquids by the means of laser irradiation”, Applied Surface Science, Vol. 247, pp. 453-457

Hiemenz P.C., Rajagopalan R., 1997. “Principles of Colloid and Surface Chemistry”, Marcel Dekker, pp. 462-465

Jagielski J., Piatkowska A., Aubert P., Thomé L., Turos A., Abdul Kader A., 2006. “Ion implantation for surface modification of biomaterials”, Surface & Coating Technology, Vol. 200, pp. 6355-6361

Katti K.S., 2004. “Biomaterials in total joint replacement”, Colloids and Surfaces B: Biointerfaces, Vol. xxx, pp. xxx-xxx

Li T.S., Li H., Pan F., 2001. “Microstructure and nanoindentation hardness of Ti/TiN multilayered films”, Surface & Coating Technology, Vol. 137, pp. 225-229

Logothetidis S., Meletis E.I., Stergioudis G., Adjaottor A.A., 1999. “Room temperature oxidation behavior of TiN thin films”, Thin Solid Films, Vol. 338, pp. 304-313

Long M., Rack H.J., 1998. “Titanium alloys in total joint replacement – a materials science perspective”, Biomaterials, Vol. 19, pp. 1621-1639

Lugscheider E., Bobzin K., 2003. “Wettability of PVD compound materials by lubricants”, Surface & Coating Technology, Vol. 165, pp. 51-57

Mandl S., Sader R., Thorwarth G., Krause D., Zeilhofer H-F., Horch H.H., Rauschenbach B., 2003. “Biocompatibility of titanium based implants treated with plasma immersion ion implantation”, Nucl. Instrum. Methods. B., Vol. 206, pp. 517-521

Marques P.A.A.P., Serro A.P., Saramago B.J., Fernandes A.C., Magalhãesa M.C.F., Correia R.N., 2003. “Mineralisation of two calcium phosphate ceramics in biological model fluids”, Journal of Materials Chemistry, Vol. 13, pp. 1484-1490

Melrose J.C., 1968. “Force Constants for Molecular Interactions Involving Hydrophobic Surface”, Phys. Chem. Publication,

Milošev I., Strehblow H.-H., 2003. “The composition of the surface passive film formed on CoCrMo alloy in simulated physiological solution”, Electrochimica Acta, Vol. 48, pp. 2767-2774

Mogensen K., Thomsen N., Esikilden S., Mathiasen C., Bottiger J., 1998. “A parametric study of the microstructural, mechanical and tribological properties of PACVD TiN coatings”, Surface and Coatings Technology, Vol. 99, pp. 140-146

Nishiguchi S., Nakamura T., Kobayashi M., Kim H.-M., Miyaji F., Kokubo T., 1999. “The effect of heat treatment on bone-bonding ability of alkali-treated titanium”, Biomaterials, Vol. 20, pp. 491-500

Okabe Y., Kurihara S., Yajima T., Seki Y., Nakamura I., Takano I., 2005. “Formation of super-hydrophilic surface of hydroxyapatite by ion implantation and plasma treatment”, Surface & Coating Technology, Vol. 196, pp. 303-306

Öztürk O., Türkan U., Eroğlu A.E., 2006. “Metal ion release from nitrogen ion implanted CoCrMo orthopedic implant material”, Surface & Coating Technology, Vol. 200, pp. 5687-5697

Piscanec S., Ciacchi L.C., Vesselli E., Comelli G., Sbaizero O., Meriani S., De Vita A., 2004. “Bioactivity of TiN-coated titanium implants”, Acta Materialia, Vol. 52, pp. 1237-1245

Ponsonnet L., Reybier K., Jaffrezic N., Comte V., Lagneau C., Lissac M., Martelet C., 2003. “Relationship between surface properties (roughness, wettability) of titanium and titanium alloys and cell behaviour”, Materials Science and Engineering C., Vol. 23, pp. 551-560

Quéré D., 2002. “Rough ideas on wetting”, Physica A., Vol. 313, pp. 32 – 46

Rosen M.J., 1989. “Surfactants and Interfacial Phenomena”, A Wiley-Interscience Publication, pp. 240-251

Robinson L., Isaksson J., Robinson N.D., Berggren M., 2006. "Electrochemical control of surface wettability of poly (3 alkylthiophenes)", Surface Science, Vol. 600, pp. L148–L152

Roy S., Basu S., 2002. "Improved zinc oxide film for gas sensor applications", Bull. Materials Science, Vol. 25, Issue 6, pp. 513–515

Santos O., Nylander T., Rosmaninho R., Rizzo G., Yiantsios S., Andritsos N., Karabelas A., Müller-Steinhagen H., Melo L., Boulangé-Petermann L., Gabet C., Braem A., Trägårdh C., Paulsson M., 2004. "Modified stainless steel surfaces targeted to reduce fouling-surface characterization", Journal of Food Engineering, Vol. 64, pp. 63-79

Sato M., Webster T.J., 2004. "Nanobiotechnology: implications for the future of nanotechnology in orthopedic applications", Expert Rev. Medical Devices, Vol. 1(1), pp. 105-114

Sioshansi P., Tobin E., 1996. "Surface treatment of biomaterials by ion beam processes", Surface & Coating Technology, Vol. 83, pp. 175-182

Škorić B., Kakaš D., Rakita M., Bibić N., Peruškob D., 2004. "Structure, hardness and adhesion of thin coatings deposited by PVD, IBAD on nitrided steels", Vacuum, Vol. 76, pp. 169-172

Sul Y., Johansson C., Petronis S., Krozer A., Jeong Y., Wennerberg A., 2002. "Characteristics of the surface oxides on turned and electrochemical oxidized pure titanium implants up to dielectric breakdown: the oxide thickness, micropore configurations, surface roughness, crystal structure and chemical composition", Biomaterials, Vol. 23, pp. 491-501

Sun C.-C., Lee S.-C., Dai S.-B., Fu Y.-S., Wang Y.-C., Lee Y.-H., 2005. "Surface free energy of CrN_x films deposited using closed field unbalanced magnetron sputtering", Applied Surface Science, Vol. xxx, pp. xxx

Tang S., Kwon O.-J., Lu N., Choi H.-S., 2005. "Surface characteristics of AISI 304L stainless steel after an atmospheric pressure plasma treatment", Surface & Coating Technology, Vol. 195, pp. 298-306

Tsyganov I., Maitz M.F., Wieser E., Richter E., Reuther H., 2005. "Correlation between blood compatibility and physical surface properties of titanium-based coatings", Surface & Coating Technology, Vol. 200, pp. 1041-1044

Türkan U., Öztürk O., Eroğlu A.E., 2006. "Metal ion release from TiN coated CoCrMo orthopedic implant material", Surface & Coating Technology, Vol. 200, pp. 5020-5027

Türkan U., 2004. "Biocompatibility and microstructural characterization of PVD coated and nitrogen implanted Co-Cr alloy", Material Science in IZTECH

Urkaç S.E.S., 2006. "Characterization of Ultra High Molecular Weight Polyethylene (UHMWPE) Modified by Metal-Gas Hybrid ion implantation", Material Science in IZTECH

Vencovsky P.K., Sanchez R., Branco J.R.T., Galvano M., 1998. "Enhancing corrosion resistance of PVD-coated ools", Surface & Coating Technology, Vol. 108-109, pp. 599-603

WEB_1, 2003. H&M Analytical Services, Inc., 13/11/2006.
http://www.h-and-m-analytical.com

WEB_2, 2006. Thomson Learning, 10/10/2006.
www.thomsonlearning.com.au/ chemistry/guide/unit1chemistry/s3.htm

WEB_3, 2005. HyperPhysics, 25/01/2007.
http://hyperphysics.phyastr.gsu.edu/hbase/ surten. html

WEB_4, 2005. Hatsopoulos Microfluids Laboratory, 03/12/2006.
http://web.mit.edu/nnf/ education/wettability/summerreading-2005short.pdf

WEB_5, 2006. KRÜSS tensiometers, 20/02/2007.
http://www.kruss.info/index.php?content=ttp%3A//www.kruss.info/techniques/surface_tension_e.html

WEB_6, Direct Healthcare International, 18/01/2007.
www.direct-heathcare.com/hip-replacement.htm.

WEB_7, 2007, Practicing Oil Analysis, 21/03/2007.
www.practicingoilanalysis.com/article_detail.

WEB_8, Nielsen Technical Trading, 21/03/2007.
www.nielsen.nielsen.dk/dk1skw/uk-reduktion-2.html.

WEB_9, 2007, KSV Instruments, 14/05/2007.
www.ksvltd.com/content/index/keysca.

Widner M.R., Heuberger M., Vörös J., Spencer N.D., 2001. "Influence of polymer surface chemistry on frictional properties under protein lubrication conditions: implications for hip-implant design", Tribol. Lett., Vol. 10, pp. 111-116

Wu K.-R., Wang J.-J., Liu W.-C., Chen Z.-S., Wu J.-K., 2006. "Deposition of graded TiO_2 films featured both hydrophobic and photo-induced hydrophilic properties", Applied Surface Science, Vol. 252, pp. 5829-5838

Zettlemoyer A.C., 1960. "Hydrophobic surfaces", Phys. Chem. Publication

Zhang Y.J., Yan P.X., Wu Z.G., Zhang W.W., Zhang G.A., Liu W.M., Xue1 Q.J., 2005. "Effects of substrate bias and argon flux on the structure of titanium nitride films deposited by filtered cathodic arc plasma", Wıley-VCH Verlag GmbH & Co. KGaA, Vol. 68, pp. 37-55

APPENDIX

TiN coated CoCrMo (#1) by ultrapure water at 25 °C

Θ (contact angle) degree	Frequency %
64	6
65	22
66	19
67	25
68	39
69	20
70	20
71	44
72	1
74	4

TiN coated CoCrMo (#7) by ultrapure water at 25 °C

Θ (contact angle) degree	Frequency %
65	22
66	24
67	20
68	24
69	35
70	21
71	22
72	19
73	5
74	4
75	4

CoCrMo (substrate) (#29) by ultrapure water at 25 °C

Θ (contact angle) degree	Frequency %
70	8
72	5
73	6
74	12
75	18
76	38
77	25
78	30
79	34
80	24

CoCrMo (substrate) (#44) by ultrapure water at 25 °C

Θ (contact angle) degree	Frequency %
67	23
68	23
69	22
70	38
71	24
72	48
73	9
74	9
75	4

TiN coated CoCrMo (#1) by SBF at 37 °C

Θ (contact angle) degree	Frequency %
64	4
65	7
66	9
67	12
68	16
69	28
70	28
71	25
72	27
73	15
74	17
75	8
76	3
77	1

TiN coated CoCrMo (#7) by SBF at 37 °C

Θ (contact angle) degree	Frequency %
66	4
67	3
68	12
69	18
70	21
71	14
72	24
73	29
74	15
75	27
76	12
77	19
78	2

CoCrMo (substrate) (#29) by SBF at 37 °C

Θ (contact angle) degree	Frequency %
73	2
74	5
75	27
76	25
77	31
78	32
79	41
80	31
81	4
82	2

CoCrMo (substrate) (#44) by SBF at 37 °C

Θ (contact angle) degree	Frequency %
71	7
72	11
73	24
74	22
75	41
76	44
77	17
78	22
79	5
80	7

TiN coated CoCrMo (#1) by ultrapure water at 37 °C

Θ (contact angle) degree	Frequency %
69	8
70	6
71	12
72	7
73	20
74	14
75	18
76	11
77	4

TiN coated CoCrMo (#7) by ultrapure water at 37 °C

Θ (contact angle) degree	Frequency %
69	4
70	4
71	3
72	2
73	3
74	8
75	8
76	13
77	23
78	15
79	13
80	4

CoCrMo (substrate) (#29) by ultrapure water at 37 °C

Θ (contact angle) degree	Frequency %
83	12
84	23
85	38
86	25
87	2

CoCrMo (substrate) (#44) by ultrapure water at 37 °C

Θ (contact angle) degree	Frequency %
80	3
81	4
82	14
83	29
84	23
85	21
86	6